

Clear Detection of C II after Maximum in the Normal Type Ia Supernova 2002fk

Régis Cartier^{1,2}, Mario Hamuy¹, Giuliano Pignata³, Francisco Förster¹, Paula Zelaya⁴, Gaston Folatelli⁵, Mark M. Phillips⁶, Nidia Morrell⁶, José Maza¹, Alejandro Clocchiatti⁴, Paolo Coppi², Carlos Contreras⁶, Miguel Roth⁶, Kathleen Koviak⁷, Kevin Krisciunas⁸, Luis González¹, Sergio González⁶ and Leonor Huerta¹

ABSTRACT

We present well-sampled *UBVR_IJHK* photometry of SN 2002fk starting 12 days before maximum light through 122 days after peak brightness, along with a series of 15 optical spectra from -4 to +95 days since maximum. Our observations show the presence of C II lines in the early-time spectra of SN 2002fk, expanding at 11,000 km s⁻¹ and persisting until 8 days past maximum light with a velocity of $\sim 9,000$ km s⁻¹. SN 2002fk is characterized by a small velocity gradient of $\dot{v}_{Si II} = 26$ km s⁻¹ day⁻¹. In the off-center explosion models of Maeda et al. (2010c), SNe Ia with low Si II velocity gradients are those with the ignition region oriented towards the observer. The connection between viewing angle of an off-center explosion and the presence of C II in the early time spectrum suggests that the observation of C II could be also due to a viewing angle effect. Adopting the Cepheid distance to NGC 1309 (Riess et al. 2011a), and correcting absolute magnitudes for the absolute magnitude/decline rate calibrations we obtain a value of $H_0 = 67.1 \pm 3.2$ km s⁻¹ Mpc⁻¹.

¹Departamento de Astronomía, Universidad de Chile, Casilla 36-D, Santiago, Chile

²Department of Astronomy, Yale University, New Haven, CT 06520-8101

³Departamento Ciencias Físicas, Universidad Andres Bello, Av. República 252, Santiago, Chile

⁴Departamento de Astronomía y Astrofísica, Pontificia Universidad Católica de Chile, Casilla 306, Santiago, Chile

⁵Institute for the Physics and Mathematics of the Universe (IPMU), University of Tokyo, 5-1-5 Kashiwanoha, Kashiwa, Chiba 277-8583, Japan

⁶Carnegie Institution of Washington, Las Campanas Observatory, Colina el Pino s/n, Casilla 601, Chile

⁷Carnegie Institution of Washington, 813 Santa Barbara Street, Pasadena, CA 911901, USA

⁸Department of Physics and Astronomy, Texas A&M University, 4242 TAMU, College Station, TX 77843, USA

Subject headings: supernovae: general - supernovae: individual: SN 2002fk - cosmological parameters - cosmology: observations

1. INTRODUCTION

Type Ia supernovae (SNe) have proven to be extremely useful as extragalactic distance indicators in the optical (Hamuy et al. 2006; Hicken et al. 2009; Folatelli et al. 2010) thanks to the relation between peak luminosity and decline rate (Phillips 1993), which allows the standardization of their luminosities, and in the near infrared (Wood-Vasey et al. 2008; Krisciunas et al. 2004b,c) where they behave almost as standard candles (Kattner et al. 2012). Photometric observations of SNe Ia have delivered Hubble diagrams with unrivaled low dispersions (0.15 mag), lower than any other available technique, which permits one to determine precise values for fundamental cosmological parameters, such as the Hubble constant and the deceleration parameter. It was this technique, in fact, that led a decade ago to the surprising discovery that the Universe is in a state of accelerated expansion caused by a mysterious dark energy that comprises 70% of the energy content of the Universe (Riess et al. 1998; Perlmutter et al. 1999). Measuring the equation of state parameter of the dark energy and its evolution with time constitutes one of the most important astrophysical challenges today.

Since the discovery of the accelerated expansion, extensive surveys and follow-up programs have increased the number of SNe Ia by more than an order of magnitude. Furthermore, the quality of the follow-up observations (light curves, early-time optical spectra, NIR spectra, nebular spectroscopy, polarization) has significantly increased. As a consequence of the increase in the statistical samples available and the degree of details observed, several traces of diversity have emerged within the family of SNe Ia that manifest in differences in several observables, most notably, early time velocity gradients (Benetti et al. 2004), the presence of unburned material, late-time nebular velocity shifts (Maeda et al. 2010a,c), line polarization (Leonard et al. 2005; Wang & Wheeler 2008), high-velocity components of spectral lines (Kasen et al. 2003; Thomas et al. 2004; Gerardy et al. 2004; Mazzali et al. 2005), and circumstellar line strengths (Sternberg et al. 2011; Foley et al. 2012d; Förster et al. 2012). Consequently, at this point the use of SNe Ia for the determination of cosmological parameters and the equation of state of the dark energy is becoming dominated by systematics (see e.g. Kessler et al. 2009; Conley et al. 2011). Among the most important sources of systematics is the extinction by dust in the SN host galaxies (Folatelli et al. 2010, and references therein) and our lack of understanding of the explosion mechanisms and the underlying physical processes (see e.g. Hillebrandt & Niemeyer 2000; Röpke et al. 2012).

The general picture of SNe Ia is the nuclear burning of a C+O white dwarf (WD). Oxygen is a product of the WD burning, so carbon is the unique evidence of the original composition of the star before the explosion. For this reason the amount and distribution of the unburned carbon material is fundamental to understand the burning process of the star. Until recently only a handful number of normal SNe Ia have shown carbon. Thanks to large surveys that have discovered and followed-up SNe from very early phases, carbon have been found in nearly 30% of the SNe before maximum light (Parrent et al. 2011; Thomas et al. 2011b; Folatelli et al. 2012; Silverman & Filippenko 2012b). On the other hand, carbon is commonly detected in very luminous objects with remarkably low expansion velocities. These objects are thought to be the result of super-Chandrasekhar-mass WD (Howell et al. 2006; Thomas et al. 2007; Yamanaka et al. 2009; Scalzo et al. 2010).

Additional multi-wavelength and multi-epoch observations of SNe Ia will be required to establish a scenario connecting the observed diversity among SNe Ia. Here we present a contribution to this subject through extensive optical and near-infrared observations for the normal Type Ia SN 2002fk obtained in the course of the “Carnegie Type II Supernova Survey” (CATS, hereafter) (Hamuy et al. 2009). Our optical data are complementary to the photometry published by the Lick Observatory Supernova Search (LOSS, Riess et al. 2009b; Ganeshalingam et al. 2010), and by the Center for Astrophysics Supernova Program (CfA3, Hicken et al. 2009). Here we present 15 optical spectra obtained from -3.96 to $+94.93$ days since maximum in the B -band, these spectra are complemented with the spectra obtained by the Center for Astrophysics Supernova Program (CfA, Blondin et al. 2012), and by the Berkeley Supernova Ia Program (BSNIP, Silverman et al. 2012a). Our near-infrared data provide one of the earliest near-infrared light curves for a Type Ia SNe. The exceptional coverage of the maximum of the optical and the near-infrared light curves together with the Cepheid distance recently measured by (Riess et al. 2011a, 2009a), makes of SN 2002fk one of the most suitable SNe Ia for the calibration of their optical and near-infrared luminosities and a refinement in the determination of the Hubble constant. The completeness of the light curves of SN 2002fk also gives us the opportunity to test independent methods for the determination of the reddening towards its host galaxy using a mixture of $B-V$ and V -near-IR colors. We report also optical spectroscopic observations covering 100 days of the evolution of SN 2002fk that provide clear evidence for unburned carbon. This is one of a handful well observed SNe Ia that have shown carbon lines in the pre-maximum spectra, and the only one where such lines persist several days past peak brightness. Thus, these observations provide important clues to our understanding of the explosion mechanisms for normal SNe Ia.

This paper is organized as follows: in section 2 we describe the photometric and spectroscopic observations and data reduction; in section 3 we present the photometric data and

the determination of the reddening caused by dust; in section 4 we show the spectroscopic evolution of SN 2002fk; in section 5 we calculate the Hubble constant using the photometry presented here complemented with LOSS and CfA3 photometry, and the distance to NGC 1309 (Riess et al. 2011a); we discuss our results in section 6 and present our conclusions in section 7. In an upcoming paper (Zelaya et al. 2013) we will present spectropolarimetric observations of SN 2002fk.

2. OBSERVATIONS AND DATA REDUCTION

SN 2002fk was discovered independently by Kushida, R. (2002) and by Wang & Qiu (2002) at $V \simeq 15.0$ mag on 2002 September 17.7. The supernova was located at $\alpha=03:22:05.71$ and $\delta=-15:24:03.2$ (J2000), $3.6''$ south and $12.6''$ west of the host galaxy NGC 1309 (see Figure 1). NGC 1309 is an SA(s)bc galaxy with a heliocentric recession velocity of $2,136 \text{ km s}^{-1}$ obtained from neutral hydrogen line measurements (Koribalski et al. 2004). Ayani & Yamaoka (2002) classified SN 2002fk as a Type Ia from an optical spectrum obtained on 2002 September 20.

2.1. Instrumental Settings

We obtained optical photometry of SN 2002fk with five telescopes and we used two instruments for near-IR photometry. Additionally we obtained galaxy subtraction templates with the Direct CCD camera on the du Pont telescope, and optical photometry of the local standard stars with the PROMPT telescopes. The instruments and their main characteristics are listed below.

i) Swope telescope located at Las Campanas Observatory (LCO), equipped with a CCD camera (2048×3150 array and pixel size = $0.435 \text{ arcsec pixel}^{-1}$) and $UBV(RI)_{KC}$ filters.

ii) du Pont telescope located at LCO, equipped with the Wide Field Reimaging CCD camera (WFCCD, 2048×2048 , pixel size = $0.774 \text{ arcsec pixel}^{-1}$) and $BV(I)_{KC}$ filters. We also obtained near-IR photometry with the Wide Field InfraRed Camera (WIRC) (1024×1024 array and pixel size = $0.196 \text{ arcsec pixel}^{-1}$) which was equipped with J_sH and K_s filters (Persson et al. 2002). Further, we obtained galaxy templates with the Direct CCD Camera (2048×2048 array and pixel size = $0.259 \text{ arcsec pixel}^{-1}$), the filter set was the same as that used on the Swope telescope (see Hamuy et al. 2006).

iii) Magellan Baade telescope located at LCO equipped with the Low-Dispersion Survey Spectrograph (LDSS-2) (2048×2048 array and pixel size = $0.380 \text{ arcsec pixel}^{-1}$ and

$BV(R)_{KC}$ filters) (Allington-Smith et al. 1994). We obtained near-IR J_sHK_s photometry with the Classic-Cam (256×256 NICMOS3 array with pixel size = $0.094 \text{ arcsec pixel}^{-1}$).

iv) 0.9m telescope located at Cerro Tololo Inter-American Observatory (CTIO), equipped with a CCD camera (2048×2048 array and pixel size = $0.396 \text{ arcsec pixel}^{-1}$) and $UBV(RI)_{KC}$ standard filters.

v) 1.5m telescope located at CTIO equipped with a CCD camera (2048×2048 array and pixel size = $0.440 \text{ arcsec pixel}^{-1}$) and $BV(RI)_{KC}$ filters.

vi) PROMPT 3 and PROMPT 5 are located at CTIO, and they are equipped with a CCD camera Alta U47 E2V CCD47–10 (1024×1024 array and pixel scale = $0.6 \text{ arcsec pixel}^{-1}$). The local standard stars around SN 2002fk were observed using $BV(RI)_{KC}$ filters. For more details about data reduction of the PROMPT telescopes see Pignata et al. (2011).

In Table 1 we summarize the instruments used for the spectroscopic follow-up and their main characteristics. More details about the instruments used are given in Hamuy et al. (2009).

2.2. Optical Photometry Reduction

We reduced the optical images using a custom IRAF¹ script package, as described in Hamuy et al. (2009). We processed the raw images through bias subtraction, and flat fielding. As long as sky flats were available we corrected small gradients in dome flat illumination ($\sim 1\%$). To reduce any possible galaxy contamination in our photometry we subtracted host galaxy templates from our SN images using host galaxy image templates obtained with the Direct CCD Camera on the 2.5 m du Pont telescope on 2005 February 13 after the SN had vanished. This instrument delivers a typical point-spread-function (PSF) of $0.7''$ (full width at half-maximum intensity), thus providing templates with better image quality than any of the SN+galaxy images. Differential PSF photometry was made on the galaxy-subtracted images using the sequence of local standards (Figure 1), calibrated against Landolt (1992) photometric standards observed during several photometric nights.

The Landolt stars were employed to derive the following photometric transformations from instrumental to standard magnitudes,

¹IRAF is distributed by the National Optical Astronomy Observatories, which are operated by the Association of Universities for Research in Astronomy, Inc., under cooperative agreement with the National Science Foundation.

$$U = u + ct_u (u - b) + zp_u \quad (1)$$

$$B = b + ct_b (b - v) + zp_b \quad (2)$$

$$V = v + ct_v (v - i) + zp_v \quad (3)$$

$$R = r + ct_r (v - r) + zp_r \quad (4)$$

$$I = i + ct_i (v - i) + zp_i \quad (5)$$

In these equations $UBVRI$ (left-hand side) are the published magnitudes in the standard system Landolt (1992), $ubvri$ (right-hand side) correspond to the natural system magnitudes, ct_i the color term, and zp_i the zero-point for filter i ².

These transformations were then applied to 11 pre-selected stars in the field of the SN in order to establish the sequence of local standards. In Table 2 we present the resulting optical photometry for our local sequence of standards stars. We employed three instruments for this purpose. We calibrated the local sequence using photometry observed in four photometric nights with the Swope, two nights with the CTIO/0.9-m, and, two nights with the PROMPT telescopes. We do not observe systematic magnitude differences in $BVRI$ filters among the different instruments and typical differences were around of 0.02 mag or less (Figure 4). In U -band there is sistematic difference of 0.064 mag between Swope and CTIO/0.9-m. Photometry in U -band is difficult to calibrate as a result of filter mismatches or differences in the sky transmission (i.e effective bandpass), and large systematic differences are common. So we proceeded to compute global averages for each star using the data obtained in all eight photometric nights.

Having established the photometric calibration of the SN 2002fk field, we carried out differential photometry between the SN and the local standards. For all five optical cameras we employed average color terms determined on multiple nights (listed in Table 3), solving only for the photometric zero-points. The resulting $UBVRI$ magnitudes covering 130 days of evolution of SN 2002fk are summarized in Table 4.

2.3. Near-IR Photometry Reduction

We obtained near-IR photometry from observations performed with the Wide Field IR Camera (WIRC) on the du Pont telescope (Persson et al. 2002) and Classic-Cam on the 6.5

²In the case of the LDSS-2 instrument which does not have an I filter, we used $(b - v)$ instead of $(v - i)$ in equation 3.

m Baade telescope.

WIRC has four different detectors. Usually only two of the detectors were used to observe. The observing strategy consisted in taking 5 dithered images of the object with detector 1, while detector 2 was used to take *sky* images. Then the detectors were switched, this means that the SN was then on detector 2 and detector 1 was then taking *sky* images.

The observations were reduced following standard procedures with a slightly modified version of the CSP–WIRC pipeline (written in IRAF, Hamuy et al. 2006; Contreras et al. 2010). We had to modify the pipeline to use sky images as dark and bias since these calibration images were not taken during the observations of SN 2002fk.

The pipeline first masks detectable sources in the sky frames and then combines them to create a final sky frame for each detector. Then the pipeline subtracts the final sky image from the science images to get a bias/dark/sky subtracted science frame. In order to correct for pixel to pixel gain variations we divide science images by a flat field constructed from the subtraction of a flat-off from a flat-on image and normalize the result. For nights where flats were not taken we used the best calibration images from the two closest nights. In addition to this, the pipeline masks cosmetic defects and saturated objects and combines the dithered frames from each detector to deliver a final science image per detector.

For Baade observing nights all the calibrations were taken, so we performed the standard data reduction. First we subtracted the bias and the dark from all frames. Then we created a flat field for each night subtracting the flat-off from the flat-on image and normalized the result. Finally, we corrected pixel-to-pixel variations dividing all science images by the flat fields.

We obtained galaxy subtraction templates, using the WIRC/du Pont configuration, on 2003 November 2 and 11 after the SN had vanished. We performed differential PSF photometry to the galaxy-subtracted images taken with the WIRC camera, and aperture photometry to the images taken with Classic-Cam. In the small field-of-view of the Classic-Cam only star c5 was observed along with the SN. This precluded us from subtracting the galaxy template and perform PSF photometry. We performed photometry using four near-IR local sequence stars around SN 2002fk on WIRC galaxy-subtracted images. We calibrated these four local standards stars with respect to Persson et al. (1998) standards using aperture photometry. The Persson standard star images were taken close in time and close to the SN field, so it was not necessary to correct for atmospheric extinction. Photometry of the local sequence was obtained in four photometric nights with the WIRC camera on the du Pont telescope. In Table 5 we present our J_sHK_s photometry for the local sequence along with the 2MASS magnitudes for comparison. Within the uncertainties our photometry is in good agreement

with the 2MASS values. This is an encouraging result considering that the Persson et al. (1998) system is different from the 2MASS photometric system (Skrutskie et al. 2006). Table 6 presents the resulting J_sHK_S photometry for SN 2002fk which covers 115 days of its evolution since discovery.

2.4. Spectroscopy

A total of 15 spectra of SN 2002fk were obtained, as summarized in Table 1. We obtained five spectra with the 6.5 m Magellan Baade telescope using LDSS-2. For these observations, a 300 line mm^{-1} grism blazed at 5000 Å was employed, covering from 3600 to 9000 Å with a resolution of 14 Å. Three spectra were observed with the Baade telescope using the Las Campanas Modular Spectrograph. This instrument uses a SITe 1752×572 pixel CCD with 300 line mm^{-1} grating blazed at 5000 Å. The wavelength range obtained was 3200 to 9200 Å with a resolution of 7 Å. On three times we used the 2.5 m du Pont telescope with the WFCCD instrument in its spectroscopic long-slit mode. A 400 line mm^{-1} blue grism was employed, covering the wavelength range from 3800 to 9200 Å with a resolution of 8 Å. We also obtained one spectrum with the Las Campanas Modular Spectrograph on the 2.5 m telescope, covering from 3790 to 7270 Å with a resolution of 7 Å. Additional information about the instruments and observing modes are presented in Hamuy et al. (2009).

Three of our spectra of SN 2002fk were obtained in polarimetric mode with the FORS1 instrument on the ESO VLT UT3 telescope on 2002 October 1st, 5th, and 14th. For each of the three epochs observed, four exposures were taken with the retarder plate at position angles of 0, 22.5, 45 and 67.5 degrees. The exposure times were 720 sec on October 1st, 720 sec on October 5th, and 600 sec on October 14th. Grism GRIS_300V was used with no order separation filter. This provides a dispersion of 2.59 Å pix^{-1} , and the resulting wavelength range 3300–8500 Å. The spectral resolution with a $1''$ slit was 12.25 Å, which we measured using the OI 5577 sky emission line. Additional observations of a flux standard, EG21, were performed at position angle 0 degrees to calibrate the flux level. We followed a standard data reduction procedure using IRAF. A single intensity spectrum was obtained for each epoch, combining the 4 angle spectra with two beams each, in the following way:

$$F_{tot} = \frac{\sum \frac{spec_i}{specerr_i^2}}{\sum \frac{1}{specerr_i^2}} \quad (6)$$

with $i=0, 22, 45$ and 67 . Where $spec_i$ is the sum of the two beams corresponding to ordinary and extraordinary rays, at each angle, and $specerr_i$ is the quadratic sum of the errors

per beam for each of the four angles. Here we present the intensity spectra alone, and we postpone the spectropolarimetric reduction details and results for an upcoming paper (Zelaya et al. 2013).

We checked our spectral flux calibration against photometry obtained within one day from taken the spectrum. The agreement was generally good. In our first two epochs we applied mangling in the blue to bring the spectra consistent with the photometry. The remaining spectra just were rescaled to bring them in accordance with the photometry.

Optical spectra of SN 2002fk were taken and recently published by the Center for Astrophysics Supernova Program (CfA, Blondin et al. 2012), and by the Berkeley Supernova Ia Program (BSNIP, Silverman et al. 2012a). CfA obtained 23 spectra covering from -3.34 to $+120.42$ days since maximum in B , and BSNIP obtained 5 spectra from $+7.70$ to $+149.70$ days after the maximum in B . In Figure 2 we compare our spectra (blue) taken near maximum light with the CfA (green), and the BSNIP (orange) spectra observed within one day from ours. In the first two spectra there is very small differences with the CfA spectra, but overall they are in good agreement. In Figure 3 we compare our spectra with the CfA and the BSNIP data taken at later phase, and at similar epochs. In general the agreement is good. These data will be used subsequently in our study.

3. LIGHT CURVES OF SN 2002fk

3.1. Optical Light Curves

Optical photometry of SN 2002fk have been published previously by the Lick Observatory Supernova Search (LOSS, Riess et al. 2009b; Ganeshalingam et al. 2010), and by the Center for Astrophysics Supernova Program (CfA3, Hicken et al. 2009). These data have good cadence of observations, notably LOSS observations begins -11.8 before B -band maximum. These datasets are a valuable complement to our optical photometry.

Before merging these datasets we compared the four local standard stars in common (stars c5, c6, c7, and c8). In Figure 4 we show the residuals obtained from the difference between our weighted mean and the values obtained by LOSS, and CfA3 for the four stars in common. Besides in table 7 we summarized the mean differences in magnitude, and the standard error of the mean differences for stars in common. There is a generally good agreement with the values of LOSS except in the I -band, where the LOSS magnitudes are systematically brighter by ~ 0.07 mag. The CfA3 stars are systematically brighter by ~ 0.03 mag in all bands.

Our original calibration of the local sequence was based on observations obtained during four photometric nights with the LCO/Swope telescope, as part of the CATS project (Hamuy et al. 2009). When we noticed this discrepancy with the LOSS photometry, we proceeded to obtain additional observations on two photometric nights with the CTIO/0.9-m telescope and on two photometric nights with the CTIO/PROMPT telescopes. As can be seen in Figure 4, both the PROMPT and the 0.9-m photometry are consistent with our previous Swope calibration, which gave us confidence in our Swope calibration. We adopted the weighted mean magnitude of the values obtained with LCO/Swope, CTIO/0.9-m, and CTIO/PROMPT telescopes for the stars in common with LOSS, and CfA3. And we used the LCO/Swope magnitudes for the rest of the local sequence.

We must consider in our analysis the quoted systematic error in the photometric calibration of the surveys. Ganeshalingam et al. (2010) quote 0.03 mag as the LOSS systematic error, while Hicken et al. (2009) give a value of 0.02 mag for the CfA3. We quote 0.02 mag as our systematic error. This value comes from the agreement typically better than 0.02 between the three photometric systems used by us to calibrate the standard stars (see Section 2.2). Taking the systematic error in account, the BVR differences with LOSS are less than 1σ , while differences with CfA3 are close to 1σ . The 0.07 mag difference in the I -band with LOSS is worrisome. Ganeshalingam et al. (2010) reported similar systematics differences in the I -band photometry with photometry of other SNe.

To reduce the discrepancy with LOSS in the I -band we added the offset of table 7. After adding the offset we performed a polynomial fit to the I -band light curve and the residuals decreased significantly. So we decided to add the offsets of table 7 to all the CfA3 and LOSS photometry. After adding the offsets the dispersion in the polynomial fits decreased from ~ 0.025 mag to ~ 0.015 mag in the R - and I -bands, while the dispersion in the B - and V -bands increased by 0.001 mag. The peak brightness, and the time of the peak remained consistent within the uncertainties after adding the offsets in BVR . For I -band the time of peak remained consistent, while the peak brightness decreased by 0.05. These offsets will be used subsequently in the LOSS, and CfA3 photometry.

In Figure 5 we present with filled circles our optical data of SN 2002fk, with open circles the LOSS photometry, and with open squares the CfA3 data. A polynomial fit to the B-band light curve around maximum brightness yields $B_{max} = 13.30 \pm 0.03$ mag on JD 2,452,547.8 ± 0.5 and a decline rate parameter $\Delta m_{15}(B) = 1.02 \pm 0.04$ which is close to the fiducial value adopted by Phillips et al. (1999) and Folatelli et al. (2010) for SNe Ia. Polynomial fits to the other lightcurves yield $V_{max} = 13.37 \pm 0.03$ mag on JD 2,452,548.5 ± 0.5 , $R_{max} = 13.36 \pm 0.02$ mag on JD 2,452,549.2 ± 0.5 , and $I_{max} = 13.57 \pm 0.01$ mag on JD 2,452,545.8 ± 0.5 . V and R peak roughly one day after B , and I peaks two days before

B. This is consistent with the typical behaviour of SNe Ia. Bright Type Ia’s usually show a secondary maximum in *R* and *I*, and in the near-IR bands. A polynomial fit to the secondary peaks yields $R_{2^{nd} \text{ max}} = 14.14 \pm 0.01$ on JD 2,452,568.3 \pm 0.5 and $I_{2^{nd} \text{ max}} = 14.08 \pm 0.01$ on JD 2,452,575.4 \pm 0.5.

In Figure 6 we compare *BVRI* light-curves of SN 2002fk and other SNe with similar $\Delta m_{15}(B)$. Despite their similar decline rates, we notice small yet real departures from a common photometric behavior, namely: 1) a dispersion in the rise rate, where SN 2002bo, SN 2002dj, and SN 2005cf show a faster rise times. This is consistent to what is found in Ganeshalingam et al. (2011), where HVG generally show shorter rise times; 2) a small bump in the *I*-band light curve of SN 2002fk that peaks 20 days past maximum in *B*, and around 7.5 days before the secondary peak that is usually observed in *I*; 3) small differences in the time and amplitude of the secondary peaks in *R* and *I*.

3.2. Near-IR Light Curves

In Figure 7 we show our near-IR light curves of SN 2002fk. Our observations begin 12 days before *B*-maximum, among the earliest *JHK* photometry ever obtained for a SN Ia. They extend to 102 days past maximum which is exceptional for a SN Ia (Krisciunas et al. 2004b; Wood-Vasey et al. 2008; Folatelli et al. 2010). The photometric coverage is remarkably good before and close to peak brightness, through the near-IR minimum, and at late times. The second near-IR peak, on the other hand, is not so well sampled. A polynomial fit to the J-band light curve around maximum brightness yields $J_{\text{max}} = 13.76 \pm 0.01$ mag on JD 2,452,544.3 \pm 0.5. Polynomial fits to the other lightcurves yield $H_{\text{max}} = 13.98 \pm 0.01$ mag on JD 2,452,543.5 \pm 0.5, and $K_{\text{max}} = 13.76 \pm 0.02$ on JD 2,452,544.2 \pm 0.5.

In Figure 8 we compare near-IR and *I*-band light curves of SN 2002fk, SN 2001el (Krisciunas et al. 2003), SN 2002dj (Pignata et al. 2008), SN 2005cf (Wang et al. 2009), and SN 2006dd (Stritzinger et al. 2010) normalized to peak magnitudes in each band. These are well-studied SNe with very complete optical and near-IR light curves and with similar $\Delta m_{15}(B)$ values. We also show in dotted-dashed lines the templates from Krisciunas et al. (2004b) and in dashed lines the templates from Wood-Vasey et al. (2008). In all bands SN 2002fk has a faster rise to peak than both templates. After maximum, it is evident that SN 2002fk has a more pronounced minimum in all *IJHK* bands compared with the other SNe and a deeper minimum than the Wood-Vasey et al. (2008) and Krisciunas et al. (2004b) templates. Although the secondary peak was not covered by our observations in *JHK*. The observations suggest a well defined secondary maximum, clearly distinguished from the first peak, and from the minimum between the peaks.

Kasen (2006) showed that the near-IR secondary maximum is related to the ionization evolution of the iron group elements. In particular the transition of the iron/cobalt gas from double to single ionized. In the scenario proposed by him, the mixing of ^{56}Ni outward increases the velocity extend of the iron core. This hasten the occurrence of the near-IR secondary maximum. In SN 2002fk the secondary peak does not occur earlier than in the rest SNe, so large mixing of ^{56}Ni is improbable. Besides, higher metallicity progenitors would produce higher fraction of stable iron group material (Timmes et al 2003). Kasen (2006) showed that a large amount of iron group material would produce that the recombination wave encounters the layers of iron-rich material relatively earlier, thus producing an earlier secondary maximum. Given that in SN 2002fk the secondary peak was not observed to occur earlier, large progenitor metallicity is also unlikely. In his models, he presented evidence that a high contrast between the peaks and the minima are expected in hotter (i.e. relatively large ^{56}Ni mass) SNe because the transition wave from double to single ionized Fe takes a longer time to reach the Fe core. Within this context the deep minimum observed in SN 2002fk seems to be produced by higher than normal ejecta temperature.

Although it was not observed in *JHK*, it is worth to mention the small bump in the *I*-band light curve of SN 2002fk. It peaks 20 days past maximum in *B*, and around 7.5 days before the secondary maximum. This bump could be due to asymmetries in the distribution of iron group elements. The differences in the light curves become much smaller around the secondary peak, after which all five SNe show a good agreement in their decline rates.

3.3. Reddening Determination

Given the early and complete optical and NIR light curves of SN 2002fk we can estimate the amount of dust reddening (Galactic + host galaxy) using different colors, assuming the standard Galactic extinction law of Cardelli et al. (1989).

Firstly, we estimate the reddening towards SN 2002fk from its late-time ($B - V$) colors using the standard Lira–Phillips relation (Lira 1996; Phillips et al. 1999) and obtain $E(B - V)_{Lira} = 0.066 \pm 0.019$. The slope of SN 2002fk is in good agreement with the Lira relation within the dispersion. Secondly, we use the near maximum optical colors versus decline rate relations (Phillips et al. 1999), which yields $E(B - V)_{B_{max}-V_{max}} = 0.009 \pm 0.044$ and $E(B - V)_{V_{max}-I_{max}} = 0.082 \pm 0.038$. Thirdly, we estimate the reddening using the $V - \text{NIR}$ colors by minimizing χ^2 between the observed $V - H$ and $V - K$ colors with respect to Krisciunas et al. (2004b) zero-reddening templates. From these fits we obtain $E(B - V)_{V-H} = 0.014 \pm 0.037$ and $E(B - V)_{V-K} = 0.075 \pm 0.036$. Within the uncertainties these results are consistent with the optical methods.

In table 8 we summarize our results. The weighted mean of the reddening using these five different methods is $E(B - V) = 0.057$ with a dispersion of 0.036 mag. This value is close to the measured Galactic reddening toward the SN 2002fk ($E(B - V) = 0.035$ mag, Schlafly & Finkbeiner 2011), which implies that the host galaxy reddening was low. This conclusion is consistent with the small absorption in our highest signal-to-noise spectra of Na I D interstellar lines at the redshift of the host galaxy.

3.4. Optical Colors

In Figure 9 we show dust corrected color curves of well observed “normal” SNe Ia, with similar $\Delta m_{15}(B)$ to SN 2002fk. We dereddened the color curves using the recalibrated extinction maps of Schlafly et al. (1998) presented by Schlafly & Finkbeiner (2011). We used the Lira–Phillips relation (Lira 1996; Phillips et al. 1999) to estimate their host galaxy reddening. We transformed reddening into extinction, at different filters, using the standard Galactic extinction law of Cardelli et al. (1989) with $R_V = 3.1$. In red are shown SN 1990N (Lira et al. 1998), SN 1994D (Patat et al. 1996), SN 1998aq (Riess et al. 2005), SN 2003du (Stanishev et al. 2007) which are low-velocity gradient (LVG) SNe. In magenta we show SN 2001el (Krisciunas et al. 2003) and SN 2005cf (Wang et al. 2009) both of which are LVG but showing strong high velocity Ca II lines near maximum light. Finally in blue are SN 2002dj (Pignata et al. 2008), SN 2002bo (Benetti et al. 2004), and SN 2009ig (Foley et al. 2012a) which are high-velocity gradient SNe.

In the upper left panel of Figure 9 we show the $U - B$ colors. Overall, we see an evident dispersion amounting to several tenths of magnitudes, despite all SNe having been corrected for dust reddening. Benetti et al. (2005) separated SNe Ia into three groups: high-velocity gradient (HVG) objects, consisting of SNe with $\dot{v}_{Si II} \gtrsim 70 \text{ km s}^{-1} \text{ day}^{-1}$ and $\Delta m_{15}(B) \lesssim 1.5$ mag, low-velocity gradient (LVG) objects, consisting of SNe with $\dot{v}_{Si II} \lesssim 70 \text{ km s}^{-1} \text{ day}^{-1}$ and $\Delta m_{15}(B) \lesssim 1.5$, and FAINT objects with $\Delta m_{15}(B) \gtrsim 1.5$. Before and near maximum the LVG SNe, shown in red, display the bluest colors. In magenta are the LVG SNe with strong high-velocity (HV) Ca II lines near maximum and among the reddest are the HVG SNe shown in blue. What is more remarkable is the difference in shape between the two most complete $U - B$ color curves. While the SN 1998aq color grows steadily redder during the first 30 days, SN 2005cf shows a dramatic blueing at early epochs, followed by an upturn seven days before maximum. The evolution of SN 2002fk is similar to SN 1994D, evolving with a linear trend from very blue $U - B$ colors at pre-maximum epochs to redder colors at about 30 days past maximum. It is important to note at this point, that even though the dispersion in $U - B$ colors can be significantly affected by systematic errors in dust

reddening corrections, the differences in shape cannot be accounted by this effect. Although filter transmission variations can reach a few tenths of a magnitude in the U -band, the differences observed at early epochs reach even one magnitude, so we believe they are real and not a result of filter mismatches or sky transmission.

The upper right panel of Figure 9 shows the $B - V$ colors. Overall, the $B - V$ color evolution of SN 2002fk is that of a normal Type Ia. As a reference we show with solid line the Lira law. At these epochs we see a small but significant dispersion at the level of ~ 0.08 mag. The four SNe with the earliest observations (SN 1994D, SN 2002bo, SN 2005cf, SN 2003du, and SN 2009ig) all show clear evidence for an upturn around 5 days before maximum that indicates an evolution from red to blue at the very early epochs. Perhaps this is a generic feature of SNe Ia but the sample is still too small to tell. This behavior was noted by Hamuy et al. (1991) in SN 1981D, based on early-time observations obtained with photographic plates (see their Fig. 5).

The $V - R$ colors are shown in the lower left panel of Figure 9. The $V - R$ color evolution of SN 2002fk has a normal shape compared to the other SNe. However, we see an intrinsic scatter at the level of 0.4 mag among the different objects, with SN 2002fk and SN 1998aq being among the reddest objects. SN 2005cf and SN 2001el, which are LVG objects with strong HV Ca II lines, are in the middle of the distribution, while the HVG objects are among the bluest objects. This apparent gradient in $V - R$ color is specially noticeable 10 days before B maximum. At later times this gradient still seems to be present, but there is more scatter in the photometry.

In the lower right of Figure 9 we show the $V - I$ colors. Although the overall shape is similar past maximum, we see evidence for a divergent behaviour at the very earliest epochs. We can separate the SNe in two groups before maximum; the SN 2002fk-like SNe which are the LVG SNe without strong Ca II before maximum, that show a steady evolution from red to blue; the SN 2005cf-like group, which are the LVG SNe with strong Ca II lines; and the HVG SNe, that show a downturn at day ~ -7 . At about ten days before maximum, the former are nearly 0.3 mag redder than the latter. An interesting case is SN 2009ig which is in the HVG group (Foley et al. 2012a) and is slightly redder than SN 2005cf, but at ~ -15 days shows redder colors than the rest SN 2005cf-like objects.

The early-time dichotomy observed in $V - I$ is reminiscent of what happens in $U - B$. Interestingly, both the U and I bands share the presence of Ca II lines, namely the Ca II H&K lines at 3951 Å and the Ca IR triplet at 8579 Å. However, as demonstrated by Cartier et al. (2011) the strength of the Ca II lines cannot completely explain the dichotomy observed in $U - B$ and $V - I$.

3.5. V-NIR Colors

In Figure 10 we show the dereddened $V - NIR$ colors of SN 2002fk. For comparison we show the $V - NIR$ color curves of SN 2001el (Krisciunas et al. 2003), SN 2002dj (Pignata et al. 2008), SN 2003du (Stanishev et al. 2007), SN 2005cf (Wang et al. 2009), and SN 2006dd (Stritzinger et al. 2010). These are well studied SNe with similar $\Delta m_{15}(B)$, early, and complete near-IR light curves. We corrected the colors making use of Galactic extinction maps of Schlafly & Finkbeiner (2011), and the Lira–Phillips relation to estimate host galaxy reddening. As in Section 3.4, we used the Cardelli et al. (1989) extinction law to transform from color excess to extinction in specific bandpasses.

We show in Figure 10 the $V - NIR$ templates of Krisciunas et al. (2004b). In dotted-dashed lines are shown the locus for slow decliners while dashed lines correspond to the locus of mid-range decliners. In the top panel we show the $V - J$ colors. SN 2002fk declines from blue to red colors at a similar rate as the locus of slow decliners, but is offset by ~ 0.2 mag to redder colors. At early epochs SN 2002fk is similar to SN 2002dj, SN 2003du, and SN 2006dd. After ten days since maximum SN 2002fk is similar to SN 2001el, and SN 2005cf.

The middle panel of Figure 10 illustrates the $V - H$ color curves. Here SN 2002fk fits the locus of the mid-range decliners at early epochs but after ten days SN 2002fk is bluer by ~ 0.2 mag than the template. At early times SN 2002fk has similar colors to SN 2002dj, SN 2003du, SN 2005cf, and SN 2006dd. SN 2002dj and SN 2006dd resemble the mid-range decliners template. After 10 days since maximum, the evolution of SN 2002fk continue to be similar to SN 2005cf.

$V - K$ colors are illustrated in the bottom panel of Figure 10. Although, at early epochs, SN 2002fk is slightly redder than the locus of mid-range decliners, overall it fits the template well. SN 2002dj is very similar to SN 2002fk, while SN 2001el, SN 2003du, and SN 2005cf show colors that better fit the locus of slow decliners.

4. OPTICAL SPECTRA

In Figure 11 we show fifteen optical spectra of SN 2002fk that span from four days before B maximum to 95 days past peak. Near maximum, SN 2002fk shows the characteristic Si II $\lambda 6355$ absorption, Ca II H&K lines, the Ca II near-IR triplet, the W-shaped S II lines, Si III $\lambda 4560$, along with C II $\lambda 6580$. Nugent et al. (1995) found a correlation between peak luminosity and $R(\text{Si II})$, the ratio of the intensities of Si II $\lambda 5972$ to Si II $\lambda 6355$ lines near maximum, which is interpreted as a temperature effect. For SN 2002fk we measure $R(\text{Si II}) = 0.189 \pm 0.002$, corresponding to a bright SN with a hot ejecta (see section 5, Nugent et al.

1995). Further evidence that SN 2002fk was hotter than normal can be drawn from the blue $B-V$ colors, and from the Si III $\lambda 4560$ and $\lambda 5740$ absorption lines before maximum, which are usually present in the early spectra of bright SNe.

A relatively weak yet evident absorption is present at ~ 6400 Å, which we identify as C II $\lambda 6580$. This line was previously identified by Blondin et al. (2012) on a spectrum taken -3.34 days since maximum. Support to this identification comes from two additional lines at ~ 4600 Å and ~ 7000 Å which can also be attributed to C II. Remarkably, the C II $\lambda 6580$ feature persists until several days past maximum, which is unprecedented in normal SNe Ia (see Parrent et al. 2011; Thomas et al. 2011b; Folatelli et al. 2012; Silverman & Filippenko 2012b). Otherwise, the post-maximum evolution of SN 2002fk is consistent with that of a Branch-normal Type Ia SNe (see section 4.1 below).

4.1. Temporal Evolution of the Spectra

In Figure 12 we compare the spectra of SN 2002fk with three well-observed SNe with similar $\Delta m_{15}(B)$: SN 1998aq (Branch et al. 2003), SN 2003du (Stanishev et al. 2007), and SN 2005cf (Wang et al. 2009; Bufano et al. 2009), the prototypical Branch-normal SN 1994D (Patat et al. 1996), and the super-luminous SN 2006gz (Hicken et al. 2007). We choose -4 , 0 , $+25$ and $+95$ days after maximum light as comparison epochs. All the spectra are in the host galaxy rest-frame and were reddening corrected as described in Section 3.4.

In the top-left of Figure 12 we show the spectra of SN 2002fk at ~ -4 days. The spectrum is characterized by lines of singly ionized intermediate-mass elements (Si, S, Mg, and Ca), higher-ionized lines of Si III, C II, and high-velocity Ca II H&K (blended with Si II $\lambda 3858$) or, on the other hand, only a strong Si II $\lambda 3858$ line (see Section 4.4), and NIR triplet lines. At this epoch the spectrum of SN 2002fk is similar to SN 2003du with both SNe showing strong Si III absorption lines, also the super-luminous SN 2006gz shows very remarkable Si III lines. Like SN 2002fk, SN 2006gz also shows very broad and strong C II $\lambda 6580$ absorptions, which are broader than the ones in SN 2002fk. If the HV Ca II lines are present in SN 2002fk, they are slightly stronger than the ones observed in SN 1994D, but not as remarkable as the HV Ca II lines present in SN 2005cf at this epoch.

In the top-right panel of Figure 12 we show the spectrum of SN 2002fk near maximum light. At this epoch SN 2002fk and SN 1998aq share similar spectral shape and features, and both SNe show Si III lines comparable to the lines present in SN 2006gz. Additionally, SN 2002fk shows normal Ca II, and maybe a weak HV Ca II lines. In contrast SN 2005cf shows strong HV Ca II lines. Remarkably, SN 2002fk still shows clear C II $\lambda 6580$ and $\lambda 7234$

absorption lines.

In the bottom-left of Figure 12 we show the spectrum of SN 2002fk at $\simeq +25$ days since maximum. This epoch is the beginning of the transition from photospheric to nebular phase and the spectra are becoming dominated by absorption of iron-peak elements (Fe II, Co II, Cr II, etc). The similarity of all the spectra at this epoch is impressive. However, it is interesting to mention that the Na I absorption in SN 2002fk is slightly stronger than in the others. In the bottom-right of Figure 12 we show the spectrum of SN 2002fk and other SNe at $\simeq +95$ days since maximum. At this epoch the transition from photospheric to nebular phase is almost complete, and all the spectra are very similar showing forbidden emission lines of iron elements (i.e. [Fe III], [Co III]). SN 2002fk is particularly similar to SN 1998aq, and still has a slightly stronger Na I absorption line.

4.2. Photospheric Expansion Velocity

In Figure 13 we show the photospheric expansion velocity of SN 2002fk measured from the minimum of the Si II $\lambda 6355$ line, and a comparison with other SNe Ia. The Si II $\lambda 6355$ line is thought to trace the position of the photosphere (Benetti et al. 2005). In red we plot three HVG SNe: SN 2002bo (Benetti et al. 2004), SN 2002dj (Pignata et al. 2008) and SN 2009ig (Foley et al. 2012a). In blue we show the five best observed LVG SNe: SN 1990N (Leibundgut et al. 1991), SN 1994D (Patat et al. 1996), SN 1998aq (Branch et al. 2003), SN 2003du (Stanishev et al. 2007) and SN 2005cf (Wang et al. 2009). For SN 2002fk we measure a velocity gradient of $\dot{v} = 26.3 \text{ km s}^{-1} \text{ day}^{-1}$ between -4 and $+14$ days since maximum, which falls in the low end of the distribution of SNe Ia (Benetti et al. 2005). We also measure the velocity ten days after maximum $v_{10} \sim 9,400 \text{ km s}^{-1}$. Compared to the Benetti et al. (2005) sample, SN 2002fk falls 3σ below the mean ($\langle v_{10} \rangle \sim 10,300 \text{ km s}^{-1} \pm 300 \text{ km s}^{-1}$). From \dot{v} and v_{10} we unambiguously classify SN 2002fk as a LVG SN. Note that in the sample of near-IR spectra of SNe Ia presented by Marion et al. (2003), SN 2002fk also stands out for its anomalously low velocity measured from the Mg II $\lambda 10910$ absorption.

In the inset of Figure 13 we show velocities measured from other prominent lines in the spectrum. Compared to Si II $\lambda 6355$, the Si III $\lambda 4560$, S II $\lambda 5635$, and Si III $\lambda 5740$ lines show lower velocities and higher velocity gradients, implying that they form below and recede faster into the SN ejecta. We observe that Ca II *H&K* possibly has two components (see Section 4.4 for a detailed discussion). The main photospheric absorption is located at $v \sim 11,150 \text{ km s}^{-1}$, and it shows a flat evolution compared to the Si II $\lambda 6355$. It is possible that a detached high-velocity Ca II component is observed four days before maximum with $v \sim 16,700 \text{ km s}^{-1}$, and could be observed on day $+5$ with $v \sim 15,700 \text{ km s}^{-1}$ (see Figure 11).

This is similar to the velocity evolution of the Ca II lines in HVG SNe.

Before maximum light the minimum of the C II $\lambda 6580$ absorption line is formed at higher velocities than Si II $\lambda 6355$ (i.e. at larger radii in the SN ejecta), but near maximum light and thereafter the C II absorption minimum is measured deeper in the ejecta than Si II. This means that there is a significant amount of unburned C II at the same position, in velocity space, where the intermediate mass elements (IME) are located. The absorption minimum of C II $\lambda 6580$ goes deeper in the ejecta with time, which could be due to emission coming from the red side of the Si II $\lambda 6355$ line (see Folatelli et al. 2012). Although the velocity estimation from the minimum of the C II lines has large associated uncertainties given the weakness of the lines, the fact that both C II $\lambda 6580$ and $\lambda 7234$ lines are located at roughly the same velocity suggests that our measurements are correct. Previous studies of Parrent et al. (2011) and Folatelli et al. (2012) have shown that the C II $\lambda 6580$ line is found at higher velocities than the Si II $\lambda 6355$ line, and the velocity gradient of these two lines is roughly the same (i.e. they are parallel in velocity vs time since maximum), which is different from what we observe in SN 2002fk.

4.3. Presence of Unburned Material

Nearly 30% of all SNe Ia show evidence of C II $\lambda 6580$ before maximum (Parrent et al. 2011; Thomas et al. 2011b; Folatelli et al. 2012; Silverman & Filippenko 2012b). In the middle panel of Figures 14 and 15 we present a series of spectra of SN 2002fk from -3.96 to $+7.70$ days since B -band maximum. The x-axis shows the expansion velocity measured with respect to C II $\lambda 6580$. The presence of C II is confirmed by the simultaneous detection of C II $\lambda 6580$ and $\lambda 7234$ lines at the same expansion velocities. The detection of both lines at several epochs, together with a possible detection of C II $\lambda 4745$ in our first two epochs at a similar velocity, gives us confidence in the identification of these features as C II.

Both C II $\lambda 6580$ and $\lambda 7234$ become weaker and shift to the red with time. Our latest detection of C II $\lambda 7234$ is at $+4.50$ days past B maximum while the C II $\lambda 6580$ absorption is even detectable at $+8.07$ days. Notably, this is the latest detection of C II in a normal SNe Ia and, as discussed in Section 4.2, it is a clear indication of the presence of unburned material mixed with IME's if a homologous expansion of the ejecta is assumed.

4.4. Spectra Modeling

We used SYN++ (Thomas et al. 2011a), an updated version of SYNOW (Fisher et al. 1997) written in C++, to model the spectra. We modeled our data, CfA, and BSNIP spectra from -3.96 to $+7.70$ days since maximum.

In SYN++, one computes a spectrum by specifying the location and optical depth for a given set of ions. The input parameters for SYN++ are the photospheric velocity, the optical depth, the e-folding length of the opacity profile, the maximum and minimum cut-off velocity for each ion, and the Boltzmann excitation temperature for parameterizing line strengths.

Recently Foley (2013) presented convincing evidence, however not definitive, that the absorption on the blue side of the *H&K* Ca II line could be produced by Si II $\lambda 3858$. Usually this absorption was attributed to a HV Ca II line. Here we try to test both hypotheses. To do this we adjusted a SYN++ model to all the spectra from -3.96 to $+7.70$ days since *B*-band maximum. In Figure 16 we present some examples of our models, overall they are good fits. We began our modeling by fitting only the photospheric lines, especially Si II and Ca II. The characteristic blackbody temperature (T_{phot}) in our models was $\sim 12,800$ K, and we set the excitation temperature (T_{exc}) of most of the ions at 500 K below T_{phot} . For the high ionization lines like Si III, and Fe III we set T_{exc} to be the same as T_{phot} . Then to get a good fit on the absorption on the blue side of the *H&K* line, without appeal to a HV Ca II line, we had to modify the T_{exc} of Si II. We changed the T_{exc} of Si II to around 7000 K, on SYN++ small variations around this value can change dramatically the strength of Si II $\lambda 3858$ line but not the strength of Si II $\lambda 6355$ line. On the other hand, we modeled this feature by adding a HV Ca II component with T_{exc} set equal to the rest of the ions, and we did not modify the rest of the parameters. Both approaches produce equally good models (see Figures 14, 15, and 16).

Foley (2013) approach requires less parameters, and reproduces the observations equally good. Remarkably the velocity and the optical depth of Si II were not modified to reproduce the absorption on the blue side of the *H&K* line. However, the low T_{exc} required to fit SN 2002fk in the Si II $\lambda 3858$ approach seems slightly odd for a SN with low $R(\text{Si II})$ (i.e. with hot ejecta), relatively bright, and which shows high ionization lines like Si III and Fe III. Additionally, there is strong evidence that supports the presence of HV Ca II in “normal” SNe Ia (Kasen et al. 2003; Gerardy et al. 2004; Mazzali et al 2005; Stanishev et al. 2007; Tanaka et al. 2008; Childress et al. 2013). These features are clearly observed at very early phases (~ -7 days) and on both *H&K* and Ca II IR-triplet, but near maximum they are not always easy to identify (Mazzali et al 2005). Our conclusion is that both Si II $\lambda 3858$ or HV Ca II lines produce equally good fits, and more realistic radiative transfer models

are necessary to asses which line is the responsible of the absorption on the blue side of the $H\&K$ line.

As can be seen on Figures 14 and 15 the red side of the Si II $\lambda 6355$ profile is not well fitted by only Si II on SYN++ (shown in red). To obtain a better fit to this profile we added a C II HV componet (shown in green). In the case of our spectra, which are not corrected by telluric absorption, this feature on the red side of the Si II profile could be due to the lack of these corrections. However, the CfA spectra also are better fitted adding this HV C II component. Interestingly, the HV C II is at roughly the same velocity of the HV Ca II ($\sim 16,000 \text{ km s}^{-1}$). The presence of a HV C II was previously suggested in Fisher et al. (1997), and is not completely unexpected since unburned carbon material should be present in the outer layers of SNe Ia. We flag the presence of HV C II as possible but not as certain.

5. DETERMINATION OF THE HUBBLE CONSTANT USING THE CEPHEID DISTANCE TO NGC 1309

With the Cepheid distance of Riess et al. (2011a) ($\mu_{NGC\ 1309} = 32.59 \pm 0.09$), the peak brightness, and the reddening derived in Section 3.3 it is straightforward to calculate the Hubble constant (H_0) via the formula $H_0 = 10^{0.2(M_{1.1}^{max} + 25 - \alpha)}$, where $M_{1.1}^{max}$ is the absolute magnitude of SN 2002fk corrected for $\Delta m15(B)$ and α is the corresponding zero point of the Hubble diagram. We adopted the zero point from Phillips et al. (1999) for BVI , and Kattner et al. (2012) for JH .

In Table 9 we present our results. In the first column we give the peak brightness corrected for Galactic and host galaxy reddening; in the second column the absolute magnitude; in the third column the absolute magnitude corrected for reddening and $\Delta m15(B)$ using the Phillips et al. (1999) and Kattner et al. (2012) calibrations, and in the fourth column the resulting value for the Hubble constant. The uncertainties in the H_0 values were computed from a Monte Carlo simulation.

Our Monte Carlo code calculated 10,000 simulated values of H_0 assuming a Gaussian distribution in: the peak magnitude; $E(B - V)$; $\Delta m15(B)$; the zero point and the slope of the decline rate versus luminosity relationship; and the zero point of the Hubble diagram (Phillips et al. 1999; Kattner et al. 2012). Finally, we also added a Gaussian distribution of zero mean and standard deviation equal to the intrinsic dispersion in the decline rate versus luminosity relationship.

To get the average value of H_0 coming from different filters, we fixed the distance to NGC 1309. Then we obtained a probability distribution for H_0 from 90,000 simulated values.

From these probability distributions we calculated H_0 for different filter combinations. We finally added the error in the distance to NGC 1309 in quadrature, which was calculated keeping all the parameters fixed except the distance.

The H_0 values in the optical bands (BVI) are very consistent with each other, yielding an average of $H_0 = 69.1^{+4.2}_{-4.2}$ km s⁻¹ Mpc⁻¹. The JH values are also consistent with each other with an average of $H_0 = 66.4^{+3.3}_{-3.3}$ km s⁻¹ Mpc⁻¹. There seems to be a small systematic difference in H_0 between the optical and IR, but formally speaking the difference amounts to only 0.50σ . When considering the five filters together, we obtain a weighted average of $H_0 = 67.1^{+3.2}_{-3.2}$ km s⁻¹ Mpc⁻¹.

Our value of $H_0 = 67.1 \pm 3.2$ is 1.7σ lower than that presented by Riess et al. (2011a) ($H_0 = 73.8 \pm 2.4$). Note that their sample also includes SN 2002fk. Most likely, this difference is due to the fact that SN 2002fk is brighter after $\Delta m_{15}(B)$ correction than their sample of eight calibrating SNe Ia. A lower value of H_0 than the one of Riess et al. (2011a) is obtained by Sullivan et al. (2011) combining the SNLS3 data with the full WMAP7 power spectrum, the Sloan Digital Sky Survey luminous red galaxy power spectrum (DR7), which yields $\Omega_m = 0.284^{+0.019}_{-0.019}$, $\omega = -1.021^{+0.078}_{-0.079}$, and $H_0 = 69.77^{+2.07}_{-2.07}$. In other words, there is some tension between SNLS3+WMAP7+DR7 and the high H_0 value obtained by Riess et al. (2011a). Our value of H_0 is in better agreement with SNLS3+WMAP7+DR7.

Mild tension is confirmed by the recent baryonic acoustic oscillations (BAOs) results of Mehta et al. (2012). Using the DR7 and data from WMAP7, they obtained $\Omega_m = 0.280 \pm 0.014$, and $H_0 = 69.8 \pm 1.2$ fitting a Λ CDM model, this is 0.8σ from our value. On the other hand, our value is in tension at the 1.9σ with the recent value of Freedman et al. (2012) ($H_0 = 74.3 \pm 2.1$). Freedman et al. (2012) value was obtained from observations of Cepheids, using a mid-IR calibration of the Cepheid period–luminosity relation. As final comparison our estimate is in agreement at less than 1σ from the value of $H_0 = 70.5 \pm 1.6$ obtained by Ho et al. (2012). This was yielded by studies of galaxy clustering from the SDSS–III Data Release 8 (DR8). These results implies that although SN 2002fk seems to be slightly brighter after $\Delta m_{15}(B)$ correction, the derived H_0 values obtained from its light curves are in agreement with recent studies.

To reconcile this mild tension in the measured value of H_0 , Mehta et al. (2012) and Freedman et al. (2012) allowed the number of relativistic particles (N_{rel}) to be a free parameter in their cosmological model. Both obtained consistent H_0 values (i.e. $H_0 \simeq 74$), when $N_{rel} \simeq 4$ instead of $N_{rel} \simeq 3$. The latter is the number of neutrino species.

Finally, our estimate of H_0 from JH magnitudes sheds light on a previous discussion regarding the zero-point of the Hubble diagram between Kattner et al. (2012) and

Folatelli et al. (2010). From practically the same near-IR observations they obtained a difference of 0.17 and 0.11 mag in the J and H zero-points, respectively. As mentioned by Kattner et al. (2012) this systematic difference arises from the fact of fitting template light curves to derive peak brightnesses in the NIR due to the large diversity in light curve shapes at these epochs (see Kattner et al. 2012, and references therein). Given that this is so critical for NIR light curves beginning after maximum, we decided to adopt sample 5 (consisting of SNe observed before NIR maximum, excluding fast declining and highly reddened objects), of Kattner et al. (2012). Had we used instead the Folatelli et al. (2010) calibration, we would have obtained $H_0(J) = 60.0^{+4.6}_{-4.2}$ and $H_0(H) = 64.5^{+5.2}_{-4.9}$.

6. DISCUSSION

Our study reveals the following distinguishing properties of SN 2002fk:

- The presence of Si II 6355 with a relatively low (9,500 km s⁻¹) expansion velocity near maximum, and a small velocity gradient, $\dot{v}_{Si II} = 26$ km s⁻¹ day⁻¹.
- The presence of C II lines in the early-time spectra expanding at 11,000 km s⁻¹ persisting until 8 days past maximum light with a velocity $\sim 9,000$ km s⁻¹, and a possible HV component with 16,000 km s⁻¹.
- The possible presence of a HV Ca II component in the early-time spectra expanding at $\sim 16,000$ km s⁻¹ persisting until 8 days past maximum. On the other hand, a strong Si II $\lambda 3858$ line is an alternative explanation for the absorption on the blue side of the $H\&K$ line (see Foley 2013).
- A low decline rate ($\Delta m_{15}(B)=1.02$) of the B lightcurve, consistent with a higher than average peak luminosity ($M_B=-19.52$).
- A slightly bluer than average $B - V$ color near maximum.
- A blue $U - B$ and a red $V - I$ early-time color, expected for LVG SNe Ia (Cartier et al. 2011).

In the off-center explosion models of Maeda et al. (2010c), SNe Ia with low Si II velocity gradients are those with the ignition region oriented towards the observer. Therefore, we expect a negative (blueshifted) velocity shifts of the [Fe II] $\lambda 7155$ and [Ni II] $\lambda 7378$ nebular lines (V_{neb}). Silverman et al. (2013) has recently shown that this is indeed the case for SN 2002fk ($V_{neb} = -2060$ km s⁻¹), lending support to the Maeda et al. (2010c) models, Cartier et al. (2011) relations (see Figure 17), and Förster et al. (2012) work. Parrent et al.

(2011) and Folatelli et al. (2012) have noted that SNe showing C II in their spectra were grouped preferentially in the bottom of the Si II expansion velocity distribution. Our observations of SN 2002fk consistent with such claims. The connection between viewing angle of an off-center explosion and the presence of C II in the early time spectrum suggests that the observation of C II could be also due to a viewing angle effect. A possible explanation could be that when the ignition region is directed towards us, the burning front leaves some pockets of unburned material in the direction to the observer. Our observations indicate also that SN 2002fk is quite luminous and somewhat bluer than normal, which might also be a signature of an ignition region oriented towards the observer.

7. CONCLUSIONS

We present early and complete optical (*BVRI*) and NIR (*JHK*) light-curves of SN 2002fk starting 12 days before maximum light through 122 days past maximum, along with a series of 15 optical spectra from -4 to +95 days since maximum.

Our observations show the presence of C II lines in the early-time spectra of SN 2002fk, expanding at $11,000 \text{ km s}^{-1}$ and persisting until 8 days past maximum light with a velocity of $\sim 9,000 \text{ km s}^{-1}$. SN 2002fk is characterized by a small velocity gradient of $\dot{v}_{Si II} = 26 \text{ km s}^{-1} \text{ day}^{-1}$, which lends support to the claim by Parrent et al. (2011) and Folatelli et al. (2012) that SNe showing C II in their spectra were grouped preferentially in the bottom of the Si II expansion velocity distribution. In the off-center explosion models of Maeda et al. (2010c), SNe Ia with low Si II velocity gradients and negative nebular velocity shifts are those with the ignition region oriented towards us. The connection between viewing angle of an off-center explosion and the presence of C II in the early time spectrum suggests that the observation of C II could be also due to a viewing angle effect.

We found a possible HV Ca II component in the early-time spectra expanding at $16,700 \text{ km s}^{-1}$ persisting until 5 days past maximum with $15,700 \text{ km s}^{-1}$, at a similar velocity of a possible detection of a HV C II component with $16,000 \text{ km s}^{-1}$. This suggest that these HV features may arise from density enhanced regions containing a mixture of Ca II and C II.

Our photometry shows good agreement with the optical magnitudes published by Riess et al. (2009b), except in the *I*-band where we find an offset of 0.07 mag that we attribute to a systematic error in their calibration. From the *B*-band light curve we measure a decline rate $\Delta m_{15}(B) = 1.02 \pm 0.04$. The observed colors yield $E(B - V) = 0.057$ with a dispersion of 0.036 mag. This value is close to the value of the Galactic reddening of

$E(B - V) = 0.035$ toward SN 2002fk (Schlafly & Finkbeiner 2011), which implies that the host galaxy reddening was low. Adopting the Cepheid distance to NGC 1309 recently measured by Riess et al. (2011a), we obtain absolute magnitudes for SN 2002fk of $M_{max}^B = -19.52 \pm 0.17$, $M_{max}^V = -19.40 \pm 0.14$, $M_{max}^I = -19.12 \pm 0.11$, $M_{max}^J = -18.88 \pm 0.09$, and $M_{max}^H = -18.64 \pm 0.09$. Correcting these for the absolute magnitude/decline rate calibrations of Phillips et al. (1999) and Kattner et al. (2012), we solve for the Hubble constant, obtaining a value of $H_0 = 67.1 \pm 3.2 \text{ km s}^{-1} \text{ Mpc}^{-1}$ which is 1.7σ lower than that presented by Riess et al. (2011a) ($H_0 = 73.8 \pm 2.4$).

We thank the anonymous referee for comments that helped to improve our work. R.C. acknowledges support by CONICYT through “Programa Nacional de Becas de Postgrado” grant D-2108082, and by the Yale-Chile fellowship in astrophysics. R.C., G.P., M.H., P.Z., F.F., J.M., A.C. acknowledge support provided by the Millennium Center for Supernova Science through grant P10-064-F (funded by “Programa Bicentenario de Ciencia y Tecnología de CONICYT” and “Programa Iniciativa Científica Milenio de MIDEPLAN”). F.F., and G.P. acknowledge support from FONDECYT through grants 3110042, and 11090421. The authors acknowledge Ryan Foley for kindly providing spectra of SN 2009ig. The research presented in this article made use of SUSPECT³ Online Supernova Spectrum Archive.

REFERENCES

- Allington-Smith et al. 1994, PASP, 703, 983
- Amanullah, R., & Goobar, A. 2011, ApJ, 735, 20
- Ayani, K., & Yamaoka, Y., 2002, IAUC 7976
- Benetti, S. et al. 2005, ApJ, 623, 1011
- Benetti, S. et al. 2004, MNRAS, 348, 261
- Blondin, S., et al. 2012, ApJ, 143, 126
- Branch, D. et al. 2003, ApJ, 126, 1489
- Bufano, F. et al. 2009, ApJ, 700, 1456
- Cardelli, J. A., Clayton, G. C., & Mathis, J. S. 1989, ApJ, 345, 245

³See <http://suspect.nhn.ou.edu/~suspect/>

- Cartier, R. et al. 2011, *A&A*, 534, L15
- Childress, M. J., Filippenko, A. V., Ganeshalingam, M. & Schmidt, B. P. 2013, arxiv.org/abs/1307.0563
- Conley, A. et al. 2011, *ApJS*, 192, 1
- Contreras, C. et al. 2010, *AJ*, 139, 519
- Fisher, A., Branch, D., Nugent, P. & Baron, E. 1997, *ApJ*, 481, L89
- Folatelli, G. et al. 2010, *AJ*, 139, 120
- Folatelli, G. et al. 2012, *ApJ*, 745, 74
- Foley, R. J. 2013, <http://arxiv.org/abs/1212.6261>
- Foley, R. J., Simon, J. D., Burns, C. R., et al. 2012d, *ApJ*, 752, 101
- Foley, R. J. et al. 2012a, *ApJ*, 744, 38
- Förster, F., González-Gaitán, S., Anderson, J., et al. 2012, *ApJ*, 754, L21
- Freedman, W. L. et al. 2012, *ApJ*, 758, 24
- Ganeshalingam, M. et al. 2010, *ApJS*, 190, 418
- Ganeshalingam, M., Li, W., Filippenko, A. V. 2011, *MNRAS*, 416, 2607
- Gerardy, C. L. et al. 2004, *ApJ*, 607, 391
- Hamuy, M. et al. 2009, *ApJ*, 703, 1612
- Hamuy, M. et al. 2006, *PASP*, 118, 2
- N. B., Schommer, R. A., Maza, J., Smith, R. C., Lira, P., & Aviles, R. 1996, *AJ*, 112, 2438
- Hamuy, M., Phillips, M. M., Maza, J., Wischnjewsky, M., Uomoto, A., Landolt, A. U., & Khatwani, R. 1991, *AJ*, 102, 208
- Hicken, M. et al. 2009, *ApJ*, 700, 331
- Hicken, M. et al. 2007, *ApJ*, 669, L17
- Hillebrandt, W., & Niemeyer, J. C. 2000, *ARA&A*, 38, 191

- Ho, S. et al. 2012, *ApJ*, 761, 14
- Howell, D. A. et al. 2006, *Nature*, 433, 308
- Kattner, S. et al. 2012, *PASP*, 912, 114
- Kasen, D. et al 2003, *ApJ*, 593, 788
- Kasen, D. 2006, *ApJ*, 649, 939
- Kessler, R. et al. 2009, *ApJS*, 185, 32
- Koribalski, B. S. et al. 2004, *AJ*, 128, 16
- Krisciunas, K. et al. 2004b, *AJ*, 127, 1664
- Krisciunas, K. et al. 2004c, *AJ*, 128, 3034
- Krisciunas, K. et al. 2003, *AJ*, 125, 166
- Kushida, R. 2002, *IAUC* 7973
- Landolt, A. U. 1992, *AJ*, 104, 340
- Leibundgut, B. et al. 1991, *ApJ*, 371, L23
- Leonard, D. C. et al. 2005, *ApJ*, 632, 450
- Lira, P. 1996, Master’s thesis, U. de Chile
- Lira, P. et al. 1998, *AJ*, 115, 234
- Maeda, K., Taubenberger, S., Sollerman, J., Mazzali, P., Leloudas, G., Nomoto, K., & Motohara, K. 2010a, *ApJ*, 708, 1703
- Maeda, K. et al. 2010c, *Nature*, 486, 82
- Mazzali, P. et al 2005, *ApJ*, 623, L37
- Marion, G. H., Höflich, P., Vacca, W. D. & Wheeler, J. C. 2003, *ApJ*, 591, 316
- Mehta, K. T., Cuesta, A. J., Xu, X., Eisenstein, D. J. & Padmanabhan, N. 2012, *MNRAS*, 427, 2168
- Nugent, P., Phillips, M., Baron, E., Branch, D. & Hauschildt, P. 1995, *ApJ*, 455, L147
- Parrent, J. T. et al. 2011, *ApJ*, 732, 30

- Patat, F., Benetti, S., Cappellaro, E., Danziger, I. J., della Valle, M., Mazzali, P. A. & Turatto, M. 1996, MNRAS, 278, 111
- Patat, F., Chandra, P., Chevalier, R., et al. 2007, Science, 317, 924
- Persson, S. E., Murphy, D. C., Krzeminski, W., Roth, M., & Rieke, M. J. 1998, AJ, 116, 2475
- Persson, S. E., Murphy, D. C., Gunnels, S. M., Birk, C., Bagish, A., & Koch, E. 2002, AJ, 124, 619
- Perlmutter, S. et al. 1999, ApJ, 517, 565
- Phillips, M. M. et al. 1999, ApJ, 118, 1766
- Phillips, M. M. 1993, ApJ, 413, L105
- Pignata, G. et al. 2011, ApJ, 728, 14
- Pignata, G. et al. 2008, MNRAS, 388, 971
- Riess, A. G. et al. 2011a, ApJ, 730, 119
- Riess, A. G. et al. 2009a, ApJ, 699, 539
- Riess, A. G. et al. 2009b, ApJS, 183, 109
- Riess, A. G. et al. 2005, ApJ, 627, 579
- Riess, A. G. et al. 1998, AJ, 116, 1009
- Röpke, F. K., Kromer, M., Seitenzahl, I. R., et al. 2012, ApJ, 750, L19
- Scalzo, R. A. et al. 2010, ApJ, 713, 1073
- Schlaafy, E. F. & Finkbeiner, D. P. 2011, ApJ, 737, 103
- Schlegel, D. J., Finkbeiner, D. P. & Davis, M. 1998, ApJ, 500, 525
- Skrutskie, M. F., et al. 2006, AJ, 131, 1163
- Silverman, J. F., et al. 2012, MNRAS, 425, 1789
- Silverman, J. F. & Filippenko, A. V. 2012, MNRAS, 425, 1917
- Silverman, J. F., Ganeshalingam, M. & Filippenko, A. V., MNRAS, (submitted)

- Simon, J. D., Gal-Yam, A., Gnat, O., et al. 2009, *ApJ*, 702, 1157
- Stanishev, V., et al. 2007, *A&A*, 469, 645
- Sternberg, A., Gal-Yam, A., Simon, J. D., et al. 2011, *Science*, 333, 856
- Stritzinger, M. et al. 2010, *ApJ*, 140, 2036
- Sullivan, M. et al. 2011, *ApJ*, 737, 102
- Tanaka, M. et al. 2008, *ApJ*, 677, 448
- Thomas, R. C. et al. 2004, *ApJ*, 601, 1019
- Thomas, R. C. et al. 2007, *ApJ*, 654, L53
- Thomas, R. C. et al. 2011a, *PASP*, 123, 237
- Thomas, R. C. et al. 2011b, *ApJ*, 743, 27
- Timmes, F. X., Brown, F. E., & Truran, J. W. 2003, *ApJ*, 590, L83
- Wang, L. & Wheeler, J. C. 2008, *ARA&A*, 46, 433
- Wang, J., & Qiu, Y.L. 2002, *IAUC* 77973
- Wang, X., et al. 2009, *ApJ*, 697, 380
- Wood-Vasey, W. M. et al. 2008, *ApJ*, 689, 377
- Yamanaka, M. et al. 2009, *ApJ*, 707, L118
- Zelaya et al. 2013, (in preparation)

Table 1. Spectroscopic Observations of SN 2002fk.

Date(UT)	JD -2,400,000	Phase (days)	Instrument/ Telescope	Wavelength Range (\AA)	Resolution (\AA)	Exposure (s)
2002 Sep 26	52543.84	-3.96	LDSS-2/Baade	3600 - 9000	14	120
2002 Sep 28	52545.89	-1.91	LDSS-2/Baade	3600 - 9000	14	200
2002 Sep 30	52547.89	0.09	WFCCD/du Pont	3800 - 9200	8	200
2002 Oct 01	52548.31	0.50	FORS1-PMOS/VLT	3330 - 8500	12	2880
2002 Oct 05	52552.32	4.50	FORS1-PMOS/VLT	3330 - 8500	12	2880
2002 Oct 08	52555.87	8.07	WFCCD/du Pont	3800 - 9200	8	200
2002 Oct 14	52561.36	13.54	FORS1-PMOS/VLT	3330 - 8500	12	2400
2002 Oct 14	52561.83	14.03	LDSS-2/Baade	3600 - 9000	14	60
2002 Oct 25	52573.15	25.35	LDSS-2/Baade	3600 - 9000	14	120
2002 Oct 29	52576.87	29.07	LDSS-2/Baade	3600 - 9000	14	90
2002 Nov 11	52589.82	42.02	Mod. Spec./Baade	3200 - 9200	7	300
2002 Nov 12	52590.83	43.03	Mod. Spec./Baade	3200 - 9200	7	200
2002 Nov 28	52606.75	58.95	Mod. Spec./Baade	3200 - 9200	7	200
2002 Dec 02	52610.70	62.90	WFCCD/du Pont	3800 - 9200	8	450
2003 Jan 03	52642.73	94.93	Mod. Spec./du Pont	3790 - 7270	7	450

Table 2. *UBRVI* Photometric Sequence Around SN 2002fk.

Star	<i>U</i>	<i>N</i>	<i>B</i>	<i>N</i>	<i>V</i>	<i>N</i>	<i>R</i>	<i>N</i>	<i>I</i>	<i>N</i>
c1	13.604(0.018)	4	13.424(0.016)	4	12.705(0.014)	4	12.322(0.015)	4	11.951(0.014)	4
c2	14.337(0.020)	4	13.386(0.016)	4	12.346(0.014)	4	11.752(0.015)	4	11.279(0.014)	4
c3	13.248(0.013)	4	13.278(0.025)	4	12.718(0.014)	4	12.366(0.016)	4	12.065(0.014)	4
c4	14.313(0.014)	4	14.230(0.019)	4	13.620(0.013)	4	13.281(0.008)	4	12.961(0.008)	4
c5	16.197(0.009)	6	16.330(0.013)	8	15.771(0.006)	8	15.424(0.007)	8	15.077(0.005)	8
c6	16.419(0.010)	6	16.437(0.013)	8	15.820(0.006)	8	15.447(0.006)	8	15.080(0.006)	8
c7	16.209(0.011)	6	16.276(0.008)	8	15.759(0.005)	8	15.429(0.010)	8	15.102(0.006)	8
c8	17.519(0.018)	6	17.555(0.013)	8	16.948(0.008)	8	16.595(0.007)	8	16.237(0.008)	8
c9	...	4	19.083(0.028)	4	17.842(0.021)	4	17.069(0.010)	4	16.425(0.007)	4
c10	...	4	16.329(0.016)	4	15.780(0.014)	4	15.425(0.015)	4	15.122(0.010)	4
c11	...	4	15.221(0.016)	4	14.669(0.014)	4	14.310(0.015)	4	14.013(0.010)	4

Note. — Uncertainties given in parenthesis, are 1σ . For each star we indicate *N*, the number of photometric nights used to calibrate them.

Table 3. Color Terms for the five Optical Cameras

Telescope	U	B	V	R	I
Swope/CCD	+0.177	+0.053	-0.054	+0.021	+0.052
du Pont/WFCCD	...	+0.125	-0.045	...	+0.010
Clay/LDDS-2	...	+0.132	+0.046
CTIO 0.9-m/CCD	+0.126	-0.086	+0.011	+0.004	+0.007
CTIO 1.5-m/CCD	+0.139	-0.080	+0.030	+0.016	+0.017

Note. — Color terms are defined in equations 1-5.

Table 4. *UBVRI* Photometry of SN 2002fk.

Date(UT)	JD-2,400,000	<i>U</i>	<i>B</i>	<i>V</i>	<i>R</i>	<i>I</i>	Telescope
2002 Sep 21	52538.8	13.523(0.013)	14.128(0.016)	14.234(0.014)	14.149(0.015)	14.119(0.010)	Swope
2002 Sep 26	52543.9	...	13.443(0.012)	13.515(0.014)	Baade
2002 Sep 30	52547.9	...	13.319(0.047)	13.358(0.019)	...	13.609(0.051)	du Pont
2002 Oct 01	52548.9	12.792(0.018)	13.287(0.016)	13.350(0.014)	13.335(0.011)	13.595(0.014)	Swope
2002 Oct 08	52555.9	...	13.675(0.076)	13.623(0.085)	...	14.003(0.074)	du Pont
2002 Oct 14	52561.8	...	14.261(0.017)	13.904(0.014)	Baade
2002 Oct 20	52567.8	15.044(0.010)	14.883(0.011)	14.239(0.010)	14.133(0.011)	14.181(0.010)	Swope
2002 Oct 21	52568.8	15.195(0.024)	15.014(0.011)	14.355(0.023)	14.139(0.013)	14.218(0.023)	Swope
2002 Oct 24	52571.9	15.544(0.017)	15.294(0.014)	14.409(0.015)	14.196(0.015)	14.198(0.015)	CTIO 0.9-m
2002 Oct 25	52572.8	15.631(0.018)	15.394(0.016)	14.500(0.014)	14.205(0.015)	14.121(0.014)	Swope
2002 Oct 29	52572.9	14.511(0.014)	Baade
2002 Oct 30	52576.9	...	15.782(0.018)	14.714(0.010)	14.376(0.014)	...	Baade
2002 Oct 08	52577.9	...	15.825(0.017)	14.778(0.019)	...	14.123(0.017)	du Pont
2002 Nov 07	52585.8	16.388(0.018)	16.238(0.016)	15.229(0.014)	14.888(0.015)	14.539(0.015)	Swope
2002 Nov 08	52586.9	...	16.277(0.016)	15.256(0.014)	14.939(0.015)	14.570(0.019)	Swope
2002 Nov 12	52590.8	16.531(0.020)	16.396(0.016)	15.440(0.014)	15.129(0.015)	14.840(0.014)	Swope
2002 Nov 18	52596.7	16.668(0.019)	16.546(0.016)	15.640(0.014)	15.358(0.015)	15.161(0.014)	Swope
2002 Dec 02	52610.7	...	16.819(0.062)	16.075(0.033)	...	15.785(0.019)	du Pont
2002 Dec 04	52612.8	17.045(0.023)	16.830(0.016)	16.091(0.014)	15.922(0.015)	15.887(0.014)	Swope
2002 Dec 07	52615.7	17.043(0.018)	16.848(0.016)	16.128(0.014)	15.981(0.015)	16.000(0.014)	Swope
2003 Jan 07	52646.7	17.803(0.024)	17.324(0.016)	16.907(0.010)	16.954(0.015)	17.184(0.014)	Swope
2003 Jan 31	52670.6	...	17.762(0.014)	17.397(0.015)	17.633(0.015)	18.069(0.027)	CTIO 1.5-m

Note. — Uncertainties given in parenthesis, are 1σ

Table 5. J_sHK_s Photometric Sequence Around SN 2002fk.

Star	J_s	J_{2MASS}	H	H_{2MASS}	K_s	K_{2MASS}
c5	14.599(0.014)	14.582(0.028)	14.259(0.008)	14.272(0.055)	14.148(0.009)	14.173(0.067)
c8	15.764(0.020)	15.712(0.062)	15.439(0.009)	15.564(0.101)	15.299(0.024)	15.408(0.179)
c12	16.093(0.011)	16.083(0.080)	15.439(0.009)	15.312(0.094)	15.190(0.019)	15.100(0.137)
c13	18.224(0.064)	...	17.628(0.077)

Note. — Uncertainties given in parenthesis, are 1σ

Table 6. J_sHK_s Photometry of SN 2002fk.

Date(UT)	JD-2,400,000	J_s	H	K_s	Telescope
2002 Sep 18	52535.7	15.162(0.011)	15.200(0.011)	15.107(0.011)	du Pont
2002 Sep 19	52536.7	14.798(0.011)	14.859(0.011)	14.797(0.011)	du Pont
2002 Sep 20	52537.8	14.540(0.011)	14.605(0.011)	14.532(0.015)	du Pont
2002 Sep 21	52538.7	14.324(0.011)	14.405(0.011)	14.323(0.011)	du Pont
2002 Sep 22	52539.7	14.132(0.011)	14.234(0.015)	14.103(0.015)	du Pont
2002 Sep 23	52540.7	14.000(0.011)	14.133(0.011)	13.997(0.011)	du Pont
2002 Sep 24	52541.7	13.860(0.016)	14.044(0.016)	13.863(0.017)	Baade
2002 Sep 24	52541.7	13.879(0.011)	14.036(0.011)	13.926(0.011)	du Pont
2002 Sep 25	52542.7	13.801(0.015)	13.975(0.011)	13.766(0.019)	Baade
2002 Sep 27	52544.7	13.764(0.015)	13.981(0.011)	13.741(0.017)	Baade
2002 Sep 29	52546.6	13.847(0.011)	14.113(0.011)	13.859(0.011)	du Pont
2002 Oct 14	52560.7	15.623(0.011)	14.590(0.011)	14.264(0.011)	du Pont
2002 Oct 15	52562.7	15.647(0.011)	14.549(0.011)	14.262(0.011)	du Pont
2002 Oct 20	52567.8	15.549(0.011)	14.332(0.011)	14.152(0.011)	du Pont
2002 Oct 23	52570.6	15.497(0.018)	du Pont
2002 Oct 24	52571.8	15.377(0.011)	14.175(0.011)	14.083(0.011)	du Pont
2002 Nov 12	52590.8	15.854(0.011)	14.905(0.011)	14.922(0.011)	du Pont
2002 Nov 14	52593.8	16.073(0.011)	15.030(0.011)	15.063(0.011)	du Pont
2002 Nov 19	52597.5	16.367(0.011)	15.248(0.011)	15.249(0.011)	du Pont
2002 Nov 22	52600.6	16.549(0.013)	15.367(0.014)	15.350(0.030)	du Pont
2002 Dec 09	52617.5	17.713(0.039)	16.112(0.015)	16.010(0.027)	du Pont
2002 Dec 11	52619.7	17.798(0.030)	16.185(0.011)	16.070(0.027)	du Pont
2002 Dec 23	52631.6	18.534(0.042)	16.797(0.017)	16.549(0.033)	du Pont
2003 Jan 11	52650.6	19.434(0.103)	17.597(0.027)	17.039(0.056)	du Pont

Note. — Uncertainties given in parenthesis, are 1σ .

Table 7. Mean Differences Between Our Photometry for the Local Standard Stars And That Obtained by LOSS^b and CfA3^c

	ΔU^a	ΔB^a	ΔV^a	ΔR^a	ΔI^a
<i>LOSS – this paper</i>	...	-0.021 ± 0.018	-0.003 ± 0.022	0.004 ± 0.029	-0.070 ± 0.024
<i>CfA3 – this paper</i>	-0.025 ± 0.026	-0.038 ± 0.010	-0.031 ± 0.008	-0.033 ± 0.007	-0.044 ± 0.006

$$^a\Delta X = mag_X^{LOSS/CfA3} - mag_X^{this\ paper}$$

^bRiess et al. (2009b); Ganeshalingam et al. (2010)

^cHicken et al. (2009)

Table 8. SN 2002fk total (Galactic + host galaxy) reddening from different methods.

Method	$E(B - V)$	Reference
$(B - V)_{Tail}$	0.066 ± 0.019	Phillips et al. (1999)
$B_{max} - V_{max}$	0.009 ± 0.044	Phillips et al. (1999)
$V_{max} - I_{max}$	0.082 ± 0.038	Phillips et al. (1999)
$(B - V)_{V-H}$	0.014 ± 0.037	Krisciunas et al. (2004b)
$(B - V)_{V-K}$	0.075 ± 0.036	Krisciunas et al. (2004b)
Mean	0.057 ± 0.036	

Table 9. Hubble constant using different filter calibrations.

Filter	m_{max}^a	M_{max}^a	$M_{1.1}^{max}{}^b$	H_0	Reference ^c
<i>B</i>	13.07(0.15)	-19.52(0.17)	-19.46(0.18)	$69.50^{+7.06}_{-6.45}$	Phillips et al. (1999)
<i>V</i>	13.19(0.11)	-19.40(0.14)	-19.35(0.15)	$71.38^{+6.19}_{-5.70}$	Phillips et al. (1999)
<i>I</i>	13.47(0.07)	-19.12(0.11)	-19.09(0.14)	$67.36^{+5.91}_{-5.29}$	Phillips et al. (1999)
<i>J</i>	13.71(0.03)	-18.88(0.09)	-18.86(0.10)	$64.18^{+4.88}_{-4.50}$	Kattner et al. (2012)
<i>H</i>	13.95(0.02)	-18.64(0.09)	-18.60(0.10)	$67.10^{+3.54}_{-3.26}$	Kattner et al. (2012)

^aMagnitude at maximum corrected for reddening (Galactic + host).

^bAbsolute magnitude at maximum corrected for reddening (Galactic + host) and $\Delta m15$.

^cReference for the $\Delta m15(B)$ and absolute magnitude relation, and the Hubble diagram zero point (the a_v of Riess et al. 2009a, 2011a).

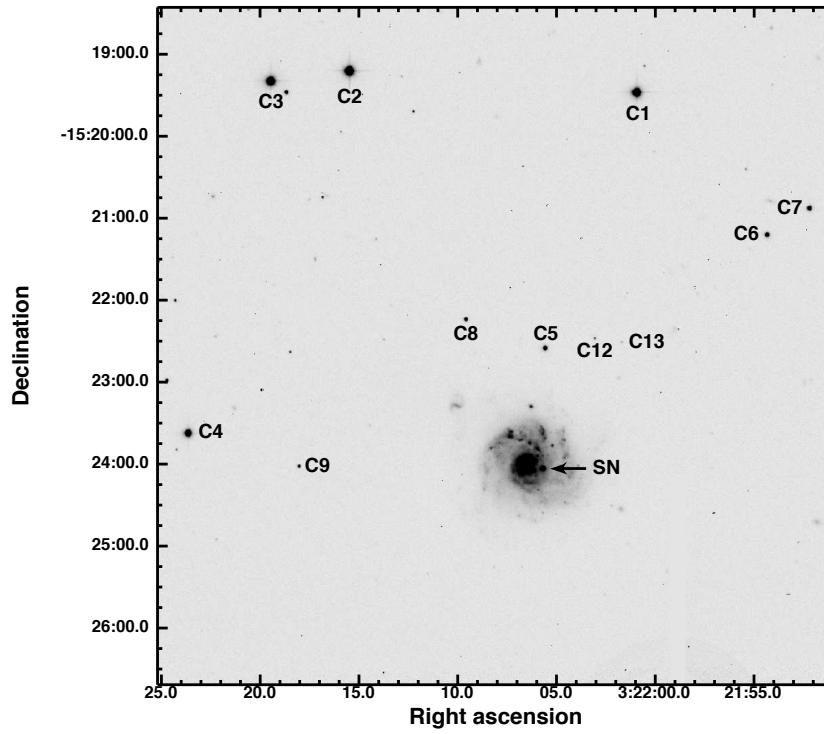


Fig. 1.— Field of SN 2002fk observed with the Swope telescope. North is up and east is to the left. SN 2002fk is marked with an arrow and eleven stars, of the local standard stars used to derive differential photometry, are labeled.

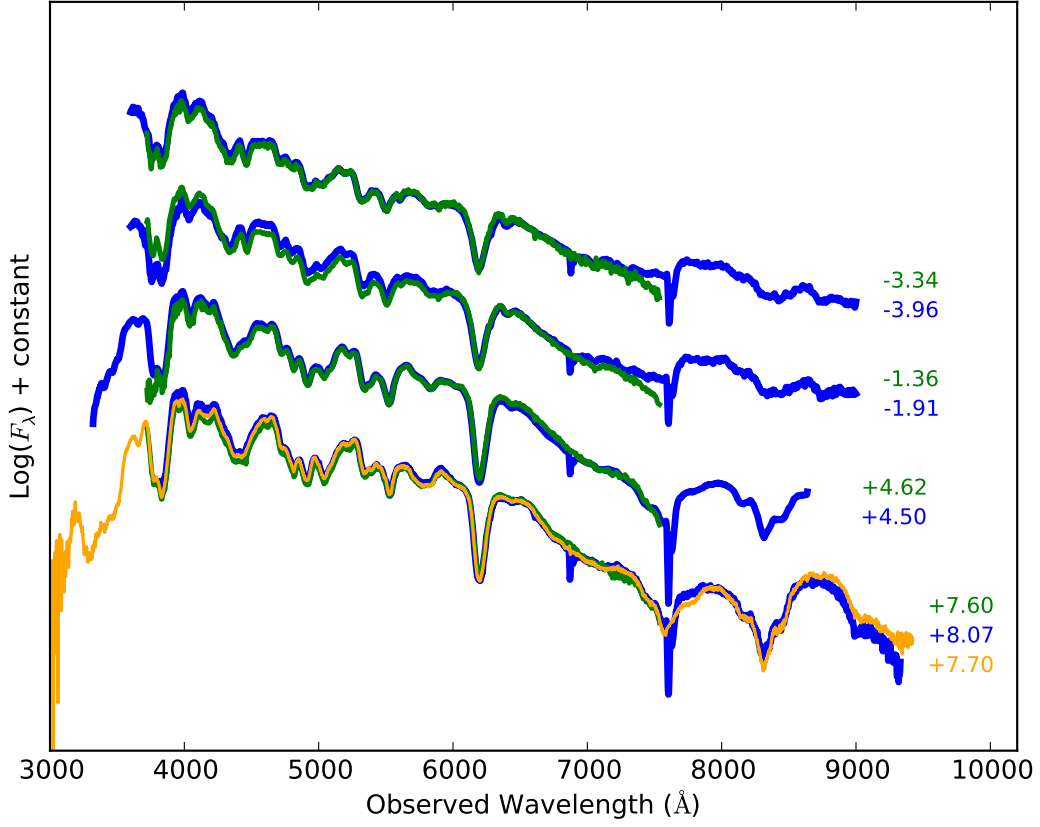


Fig. 2.— Comparison between spectra, taken near maximum light, prented here (blue), the CfA spectra (green, Blondin et al. 2012), and the BSNIP (orange, Silverman et al. 2012a) spectra observed within one day from ours. The phase is indicated on the right.

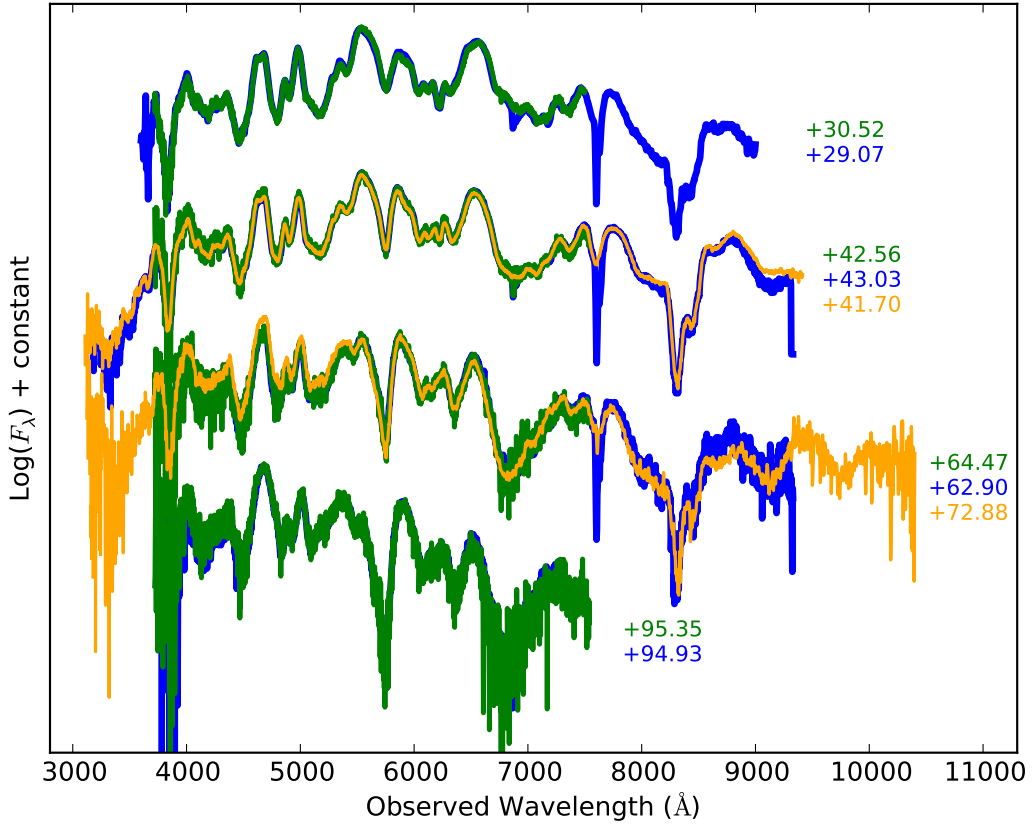


Fig. 3.— Comparison between our spectra (blue), the CfA (green, Blondin et al. 2012), and the BSNIP (orange, Silverman et al. 2012a) spectra taken at later phases, and at similar epochs. The phase is indicated on the right.

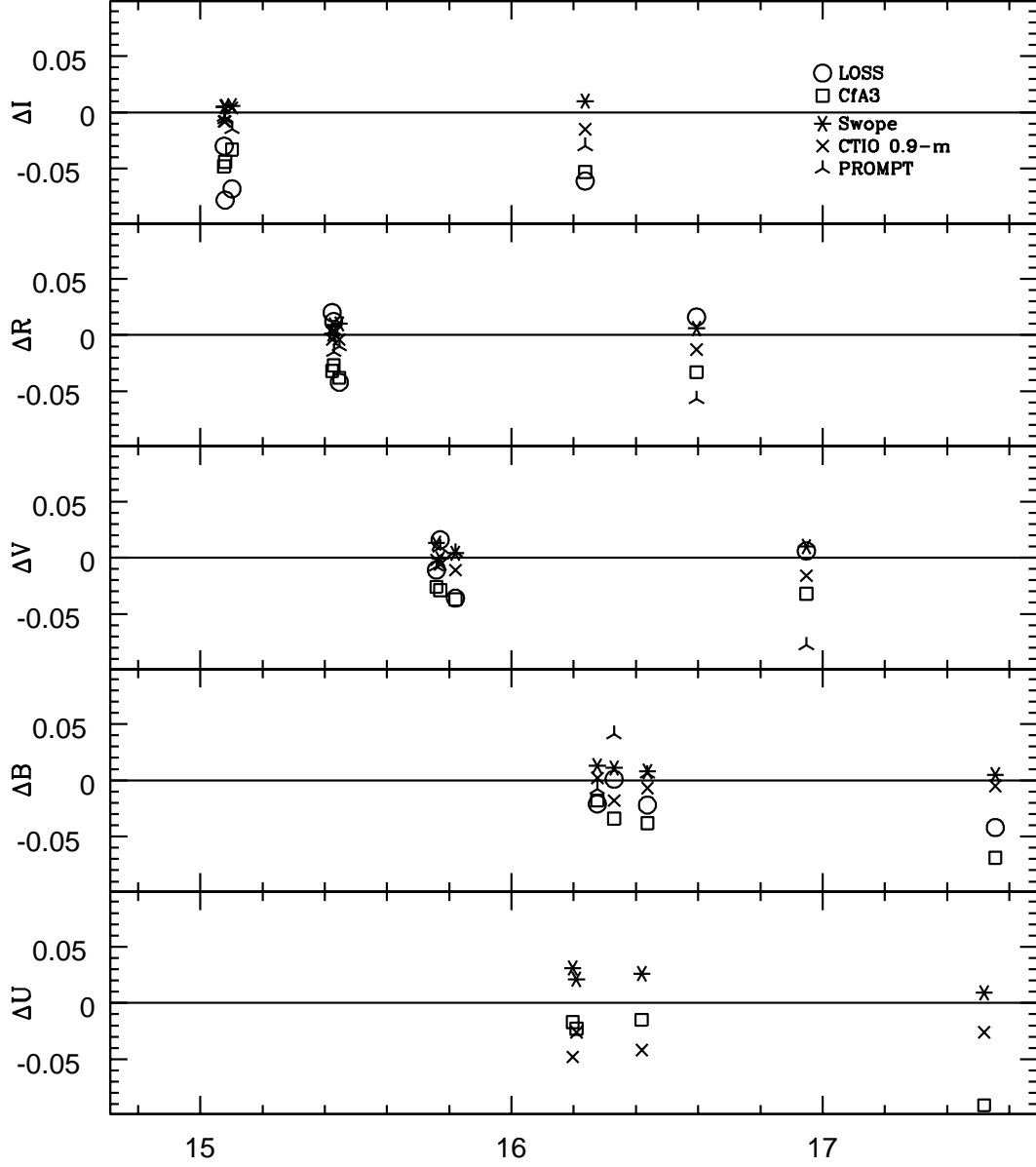


Fig. 4.— Differences between the photometry obtained with different telescopes (Swope, CTIO 0.9-m, and PROMPT) and the mean magnitudes presented here for the local standard stars in common with LOSS (Riess et al. 2009b; Ganeshalingam et al. 2010), and CfA3 (Hicken et al. 2009).

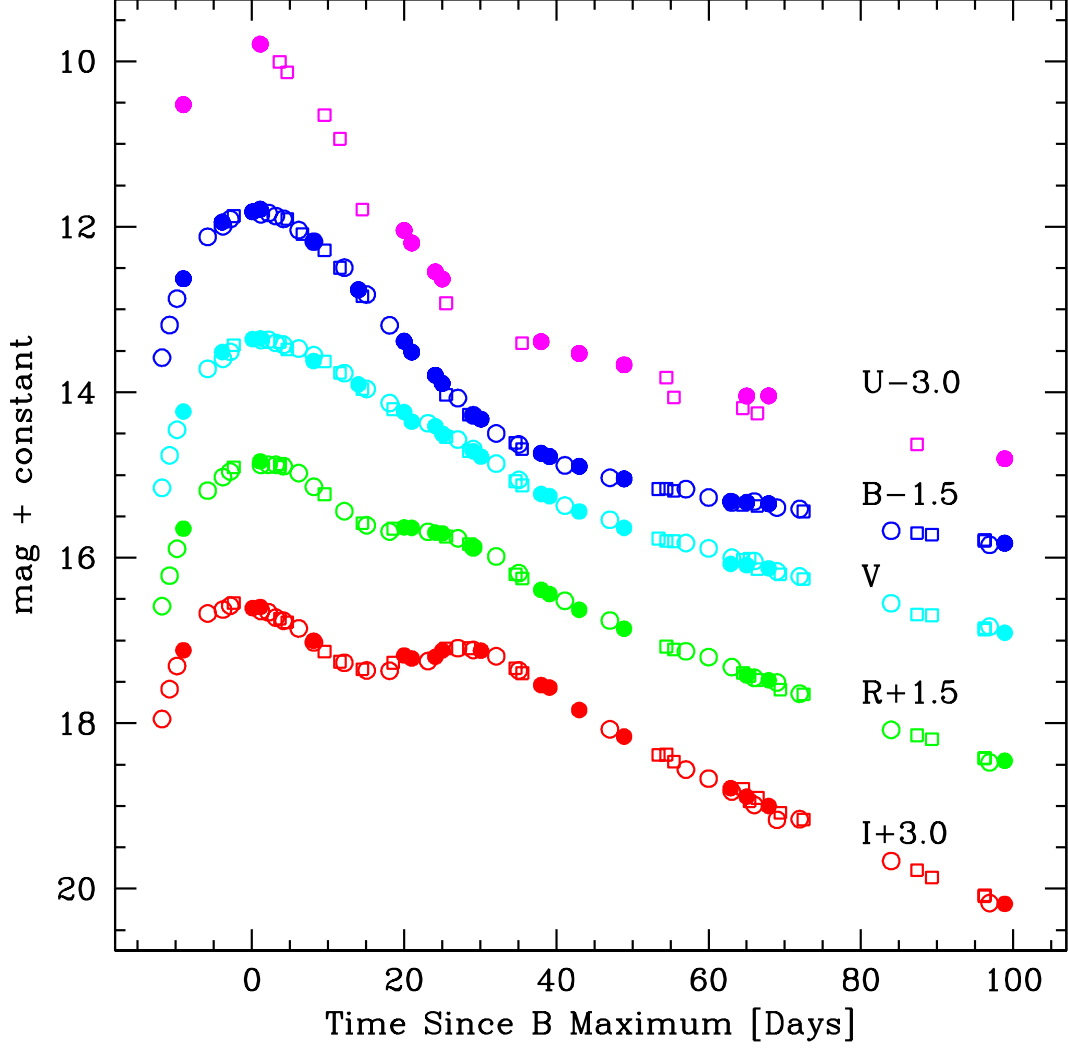


Fig. 5.— Optical light curves of SN 2002fk. Filled circles are our observations, open circles correspond to LOSS measurements, and open squares to CfA3 data. Photometry of LOSS and CfA3 were shifted by the offsets given in Table 7 to match our observations (as discussed in Sec. 3.1).

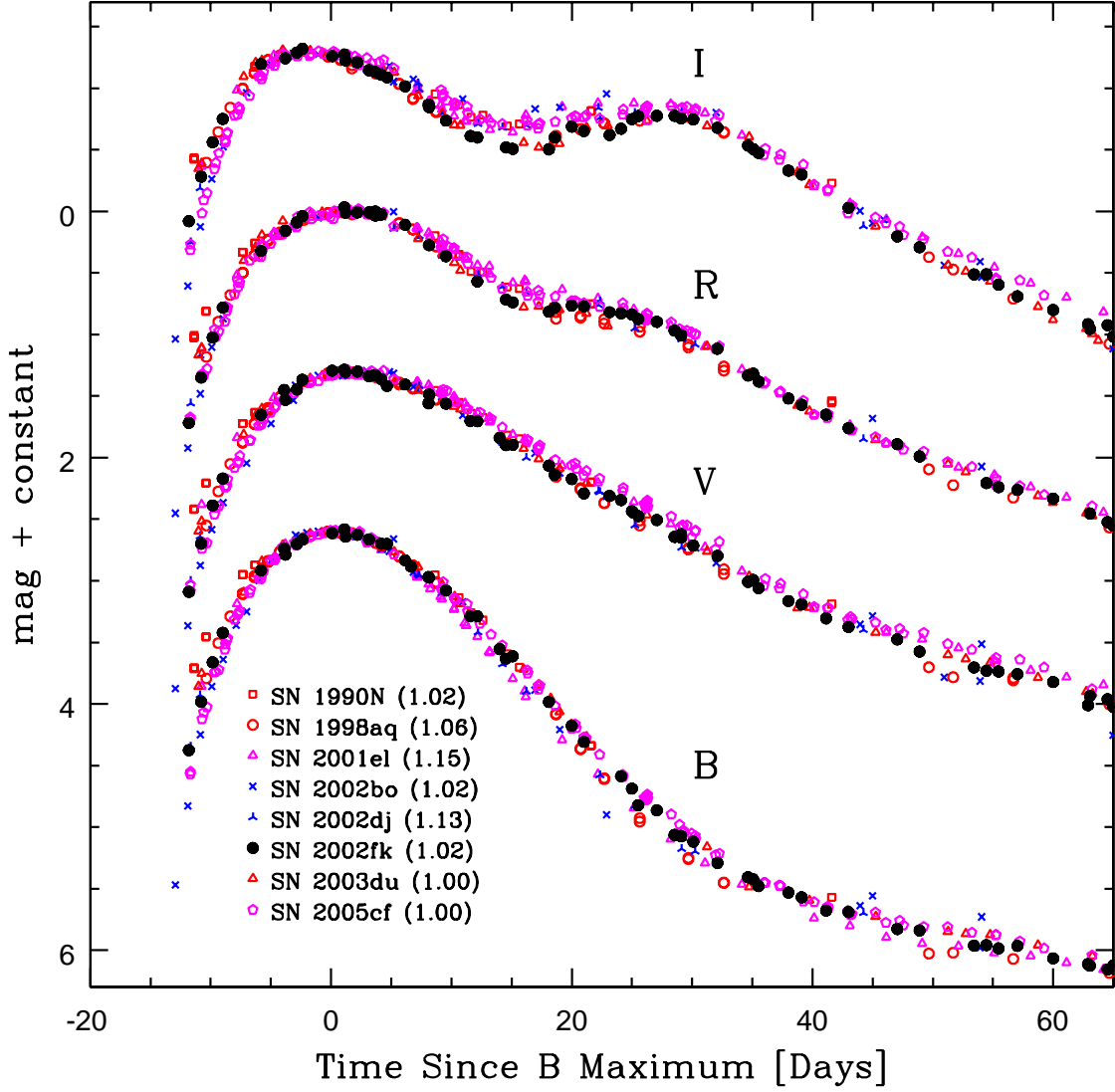


Fig. 6.— $BVRI$ light curves of SN 1990N, SN 1998aq, SN 2001el, SN 2002bo, SN 2002dj, SN 2002fk, SN 2003du, and SN 2005cf, (Lira et al. 1998; Riess et al. 2005; Krisciunas et al. 2003; Benetti et al. 2004; Pignata et al. 2008; Stanishev et al. 2007; Wang et al. 2009) selected for their similar decline rates, normalized to peak brightness. $\Delta m_{15}(B)$ is given in parenthesis.

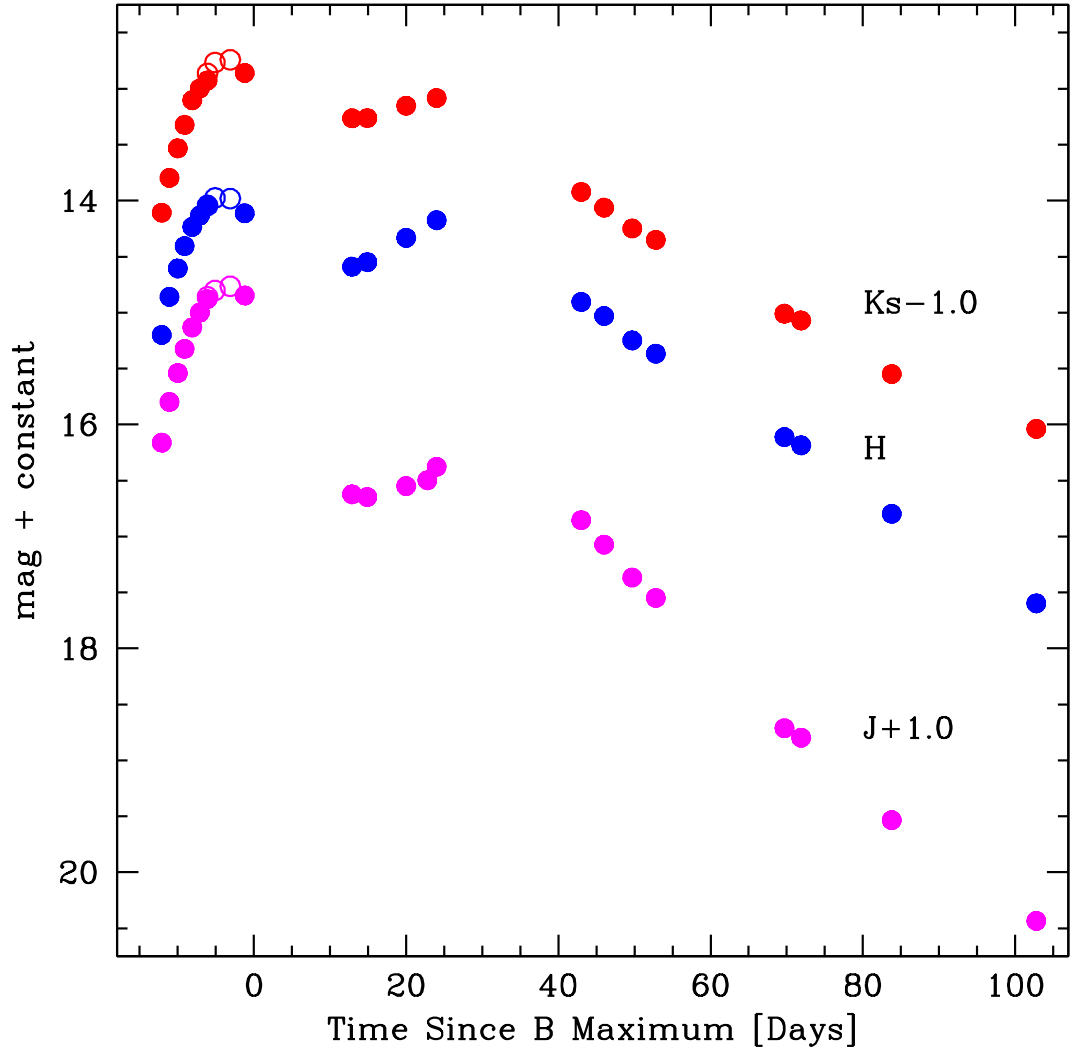


Fig. 7.— Near-IR light curves of SN 2002fk. Open symbols are data observed with Classic-Cam and filled symbols correspond to data observed with WIRC.

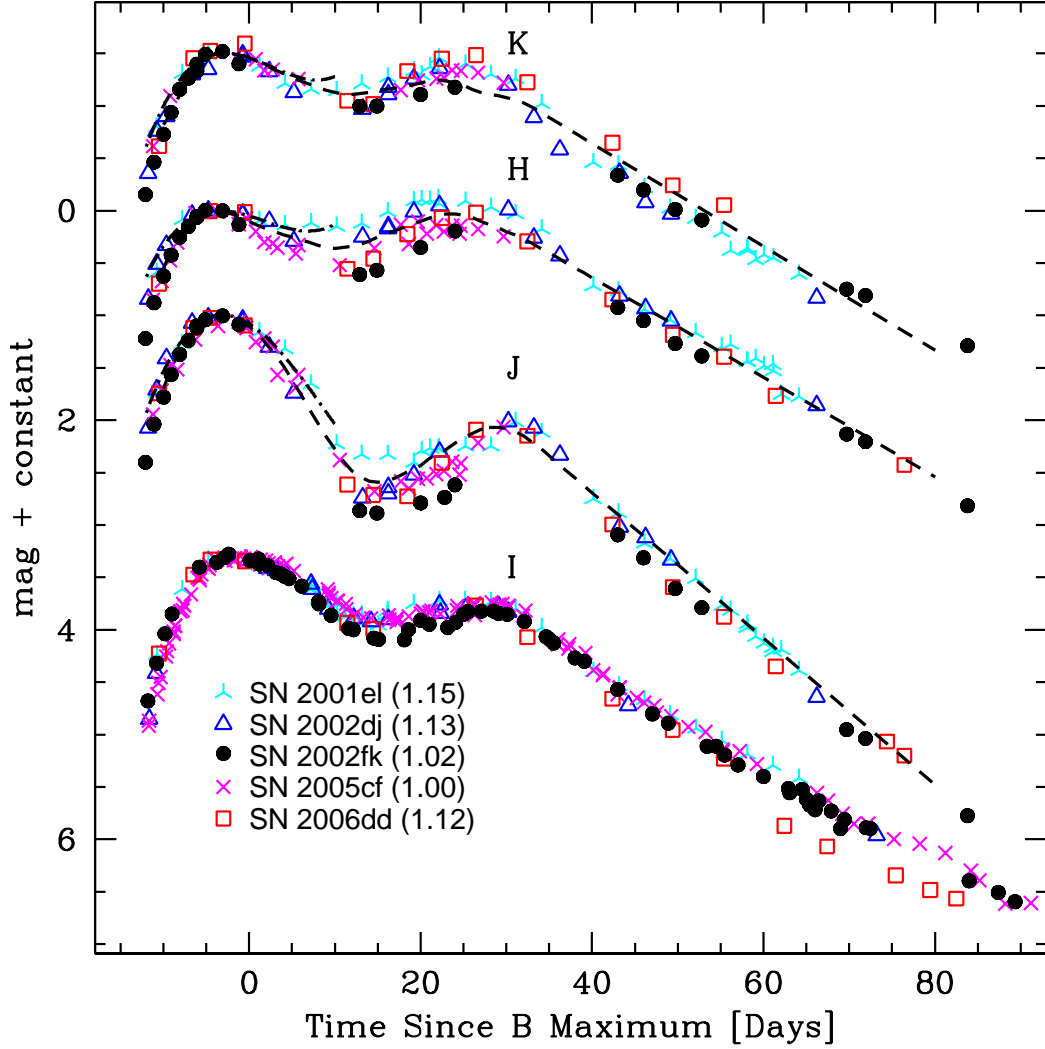


Fig. 8.— $IJHK$ light curves of SN 2001el (cyan), SN 2002dj (blue), SN 2002fk (black), SN 2005cf (magenta), and SN 2006dd (red), selected for their similar decline rates, normalized to peak brightness. We chose to compare the templates of Krisciunas et al. (2004b) (dotted-dashed line) and Wood-Vasey et al. (2008) (dashed line). $\Delta m_{15}(B)$ is given in parenthesis.

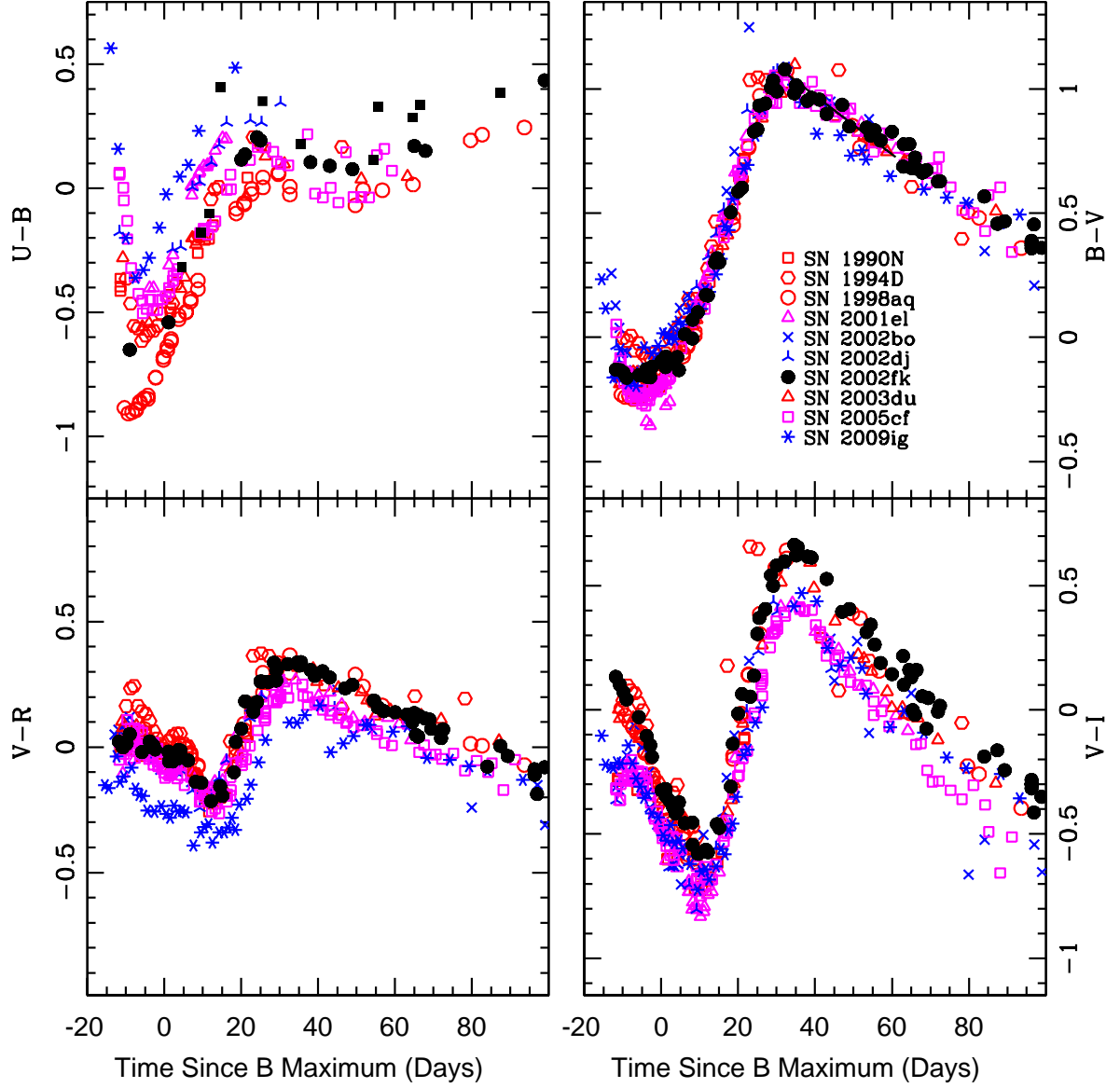


Fig. 9.— Optical colors of SN 2002fk (in black). For comparison, in red are shown the LVG SN 1990N, SN 1994D, SN 1998aq, and SN 2003du. In magenta are shown the LVG SN 2001el and SN 2005cf that show strong HV Ca II near maximum, and in blue de HVG SN 2002bo, SN 2002dj and SN 2009ig.

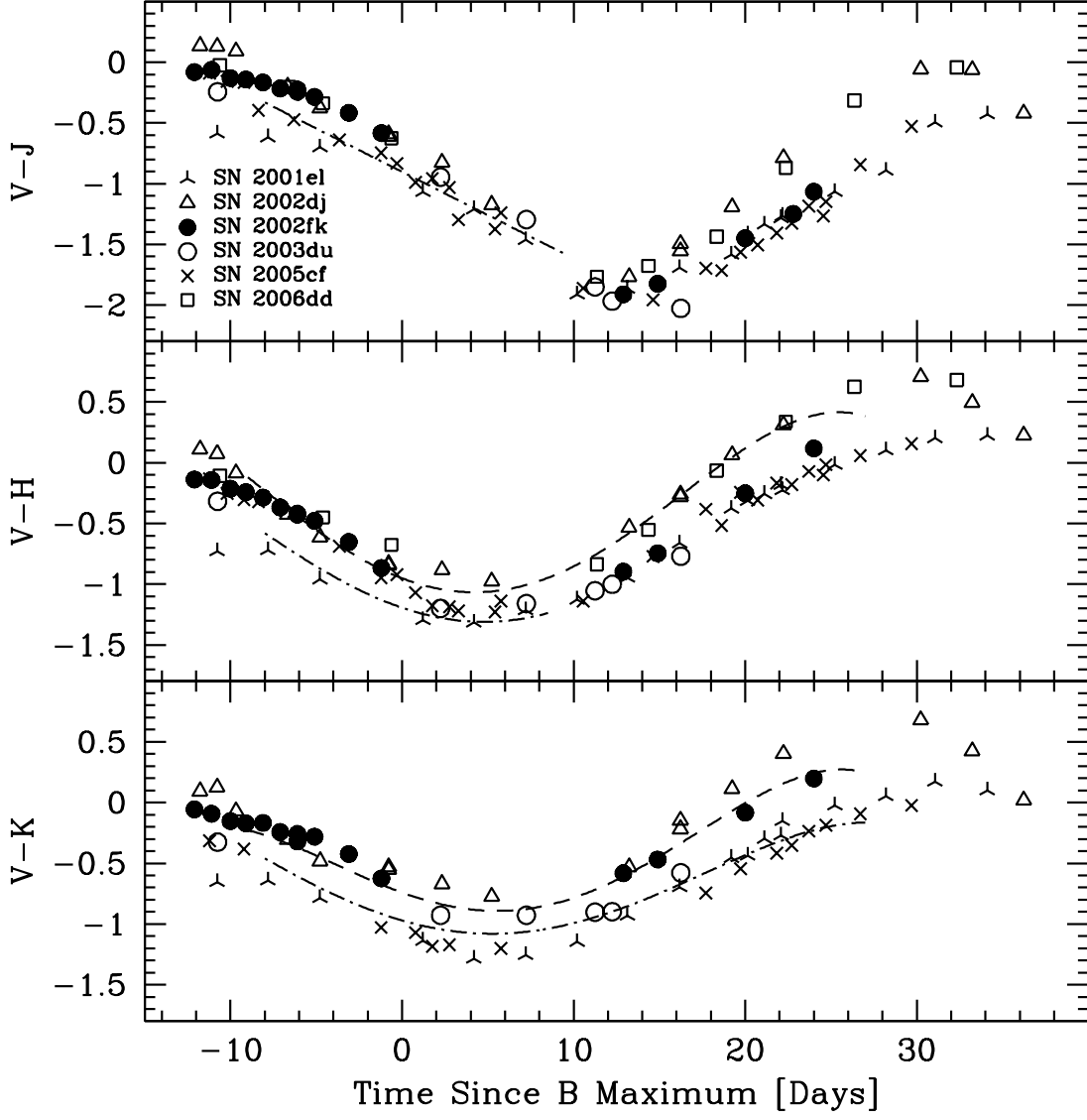


Fig. 10.— V-NIR colors of SN 2002fk and the well sampled SNe Ia of similar Δm_{15} SN 2001el, SN 2002dj, SN 2003du, SN 2005cf and SN 2006dd. Dashed line are V-NIR loci for mid-range decliners and dotted-dashed line are V-NIR loci for slow decliners (Krisciunas et al. 2004b).

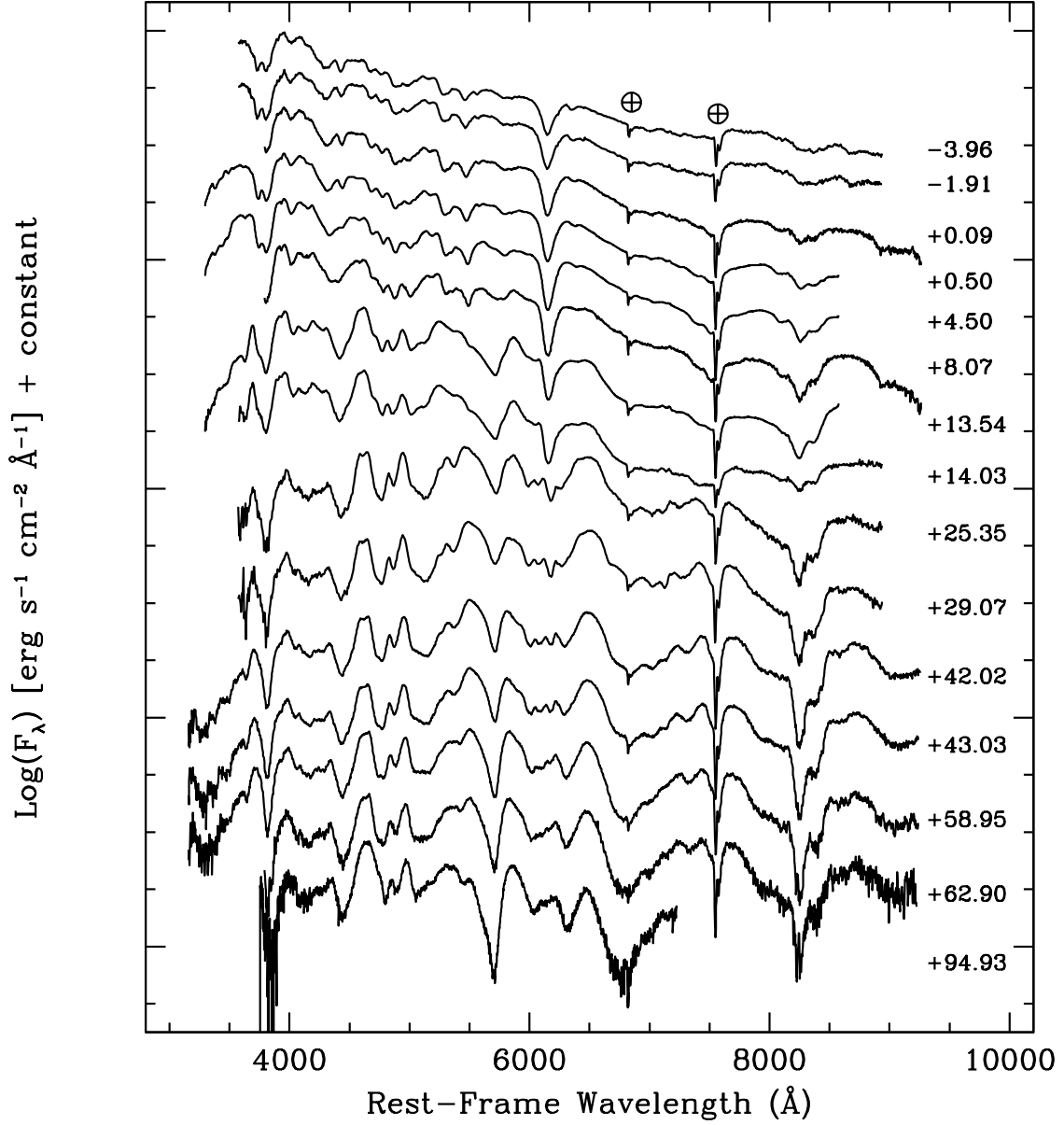


Fig. 11.— Optical spectral evolution of SN 2002fk. The spectra have been corrected for the redshift of the host galaxy ($2,137 \text{ km s}^{-1}$) and have been shifted vertically for clarity. The labels on the right mark the days since B-band maximum.

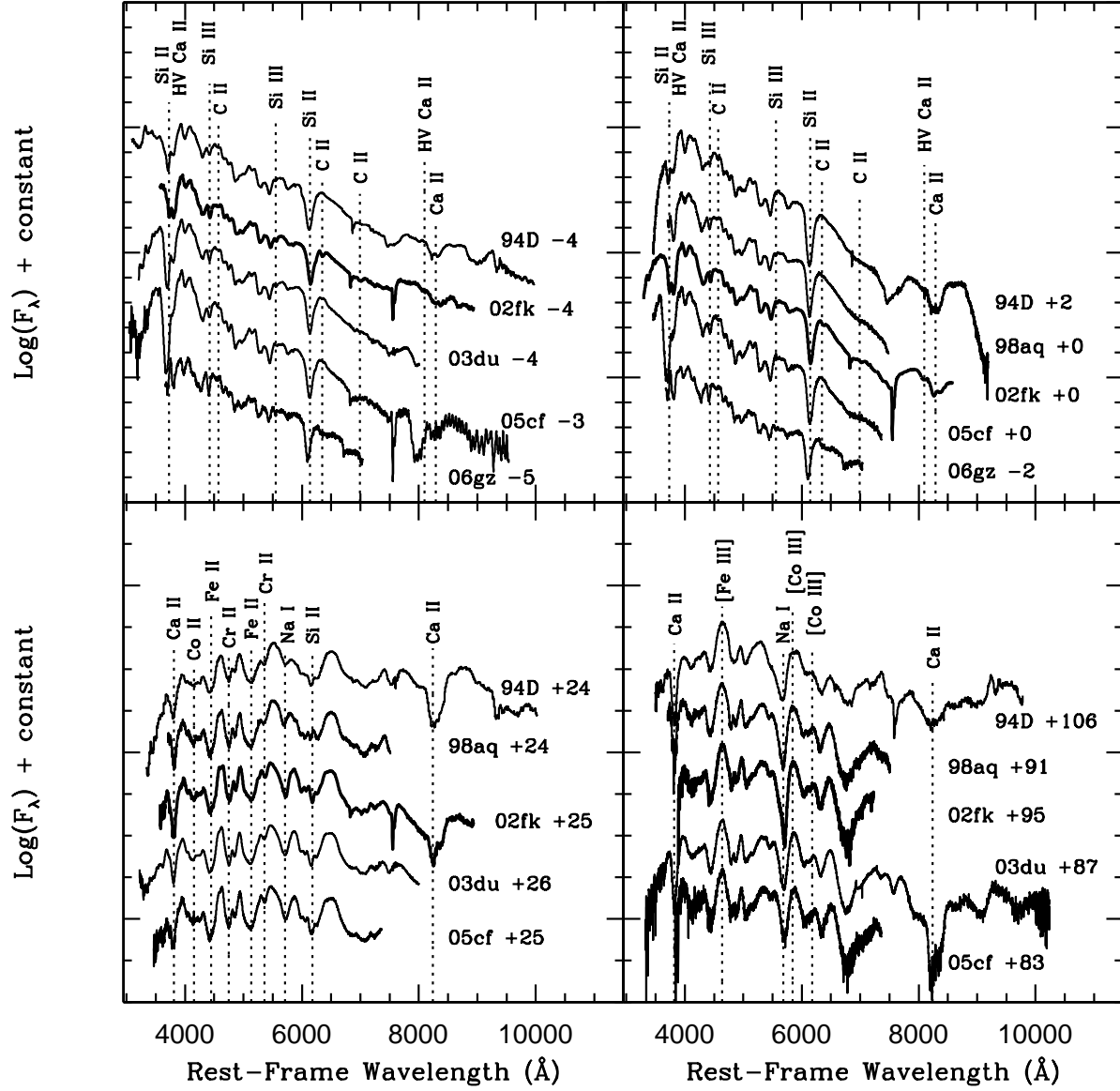


Fig. 12.— Spectrum of SN 2002fk at -4, 0, +25 and +95 days after B maximum. We plot for comparison SN 1994D, SN 1998aq, SN 2003du, SN 2006gz, and SN 2005cf at similar epochs.

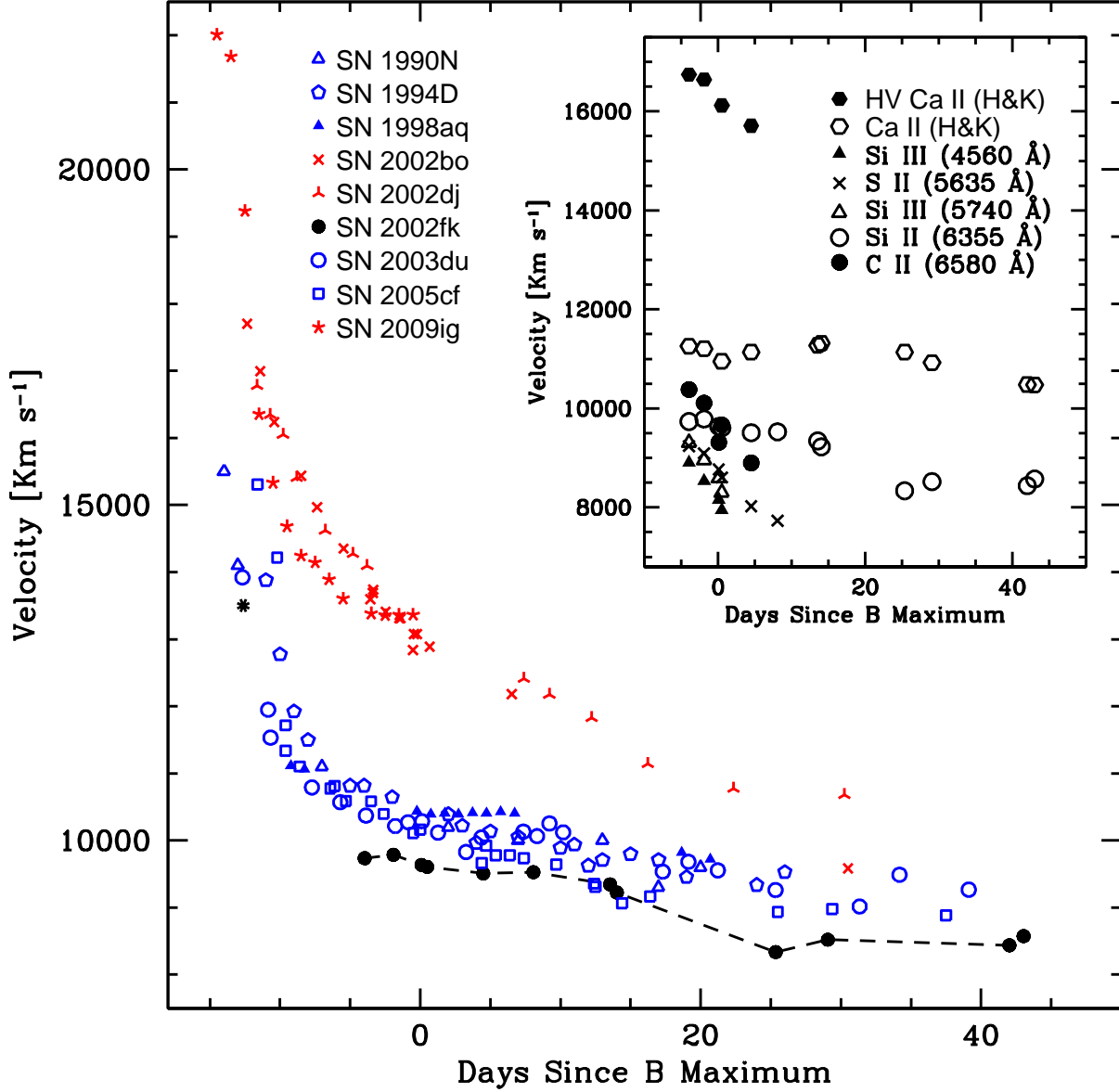


Fig. 13.— Time evolution of the photospheric expansion velocity derived from Si II $\lambda 6355$. Red symbols correspond to HVG SNe, blue symbols to LVG SNe. Black dots correspond to SN 2002fk, the black asterisk is the velocity of Si II $\lambda 16\,910$ obtained by Marion et al. (2003) from a NIR spectrum taken 12 days before maximum. In the inset we show the time evolution of other optical lines in SN 2002fk.

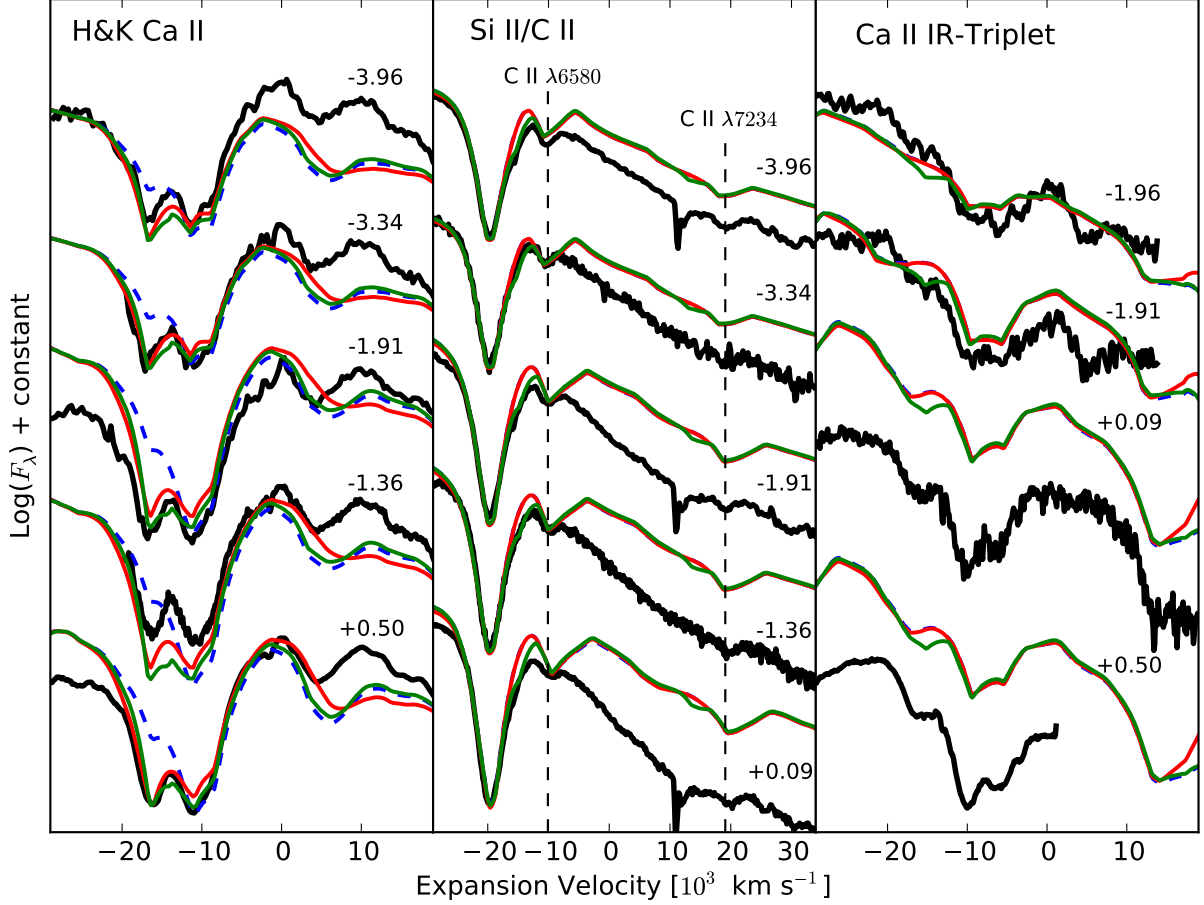


Fig. 14.— SYN++ models of the SN 2002fk spectra. Data are shown in black. Left panel: in blue-dashed we show models of $H\&K$ Ca II lines using T_{exc} close to the T_{phot} and not including a HV Ca II component. In red we show models using T_{exc} of Si II $\sim 7,000 \text{ K}$, and in green we show models using T_{exc} close to the T_{phot} and including a HV Ca II component. The x-axis is the expansion velocity measured with respect to the $H\&K$ Ca II line. Middle panel: in red we show models using T_{exc} of Si II $\sim 7,000 \text{ K}$. In green we show models using T_{exc} close to T_{phot} and including a HV C II component to get a better fit to the red side of the Si II line. The x-axis is the velocity measured with respect to C II $\lambda 6580$. Right panel: as in the left panel but for the Ca II IR-triplet. The x-axis is the expansion velocity measured with respect to the Ca II triplet. The phase of the spectra is on the right side of each panel.

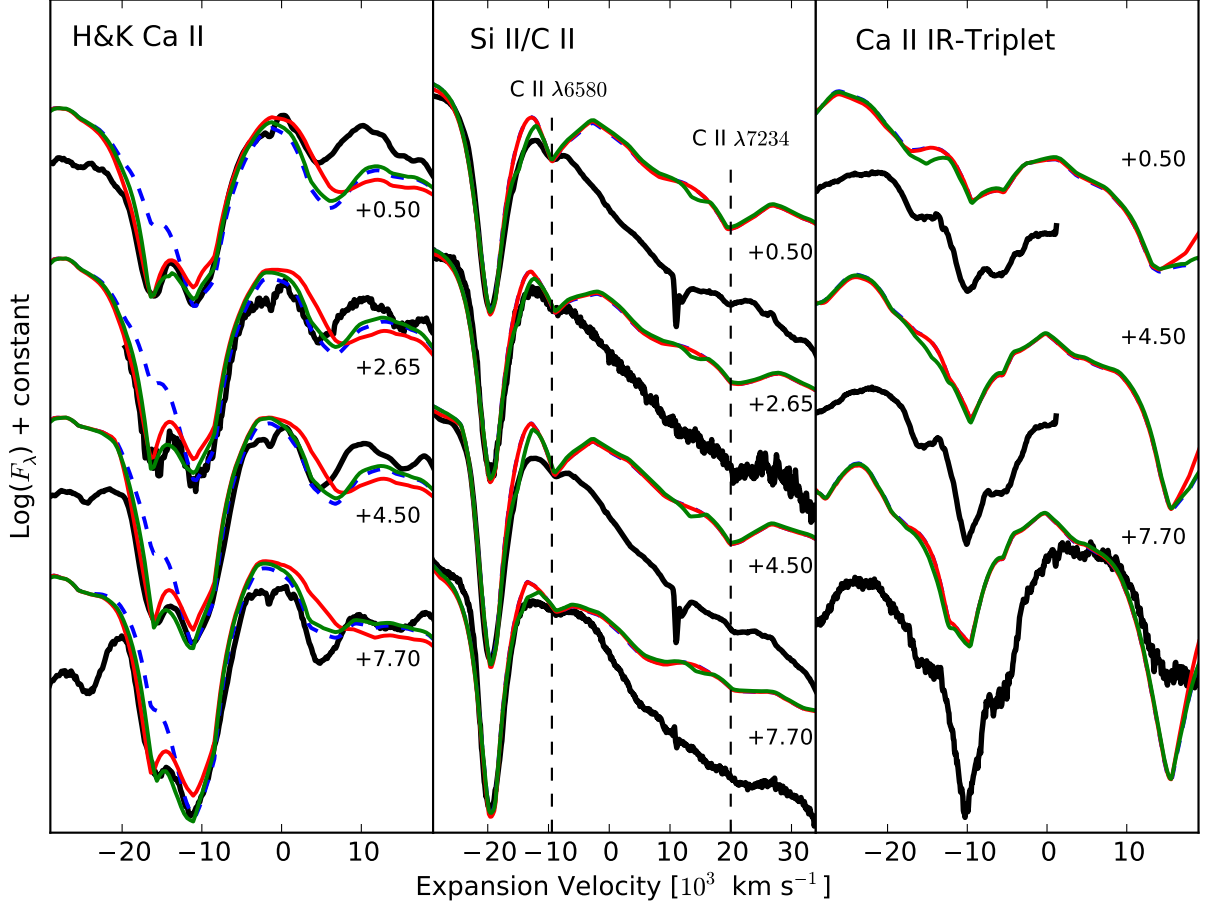


Fig. 15.— SYN++ models of the SN 2002fk spectra. Data are shown in black. In the three panels we show the same models as in Figure 14 but for later phases. The phase of the spectra is on the right side of each panel.

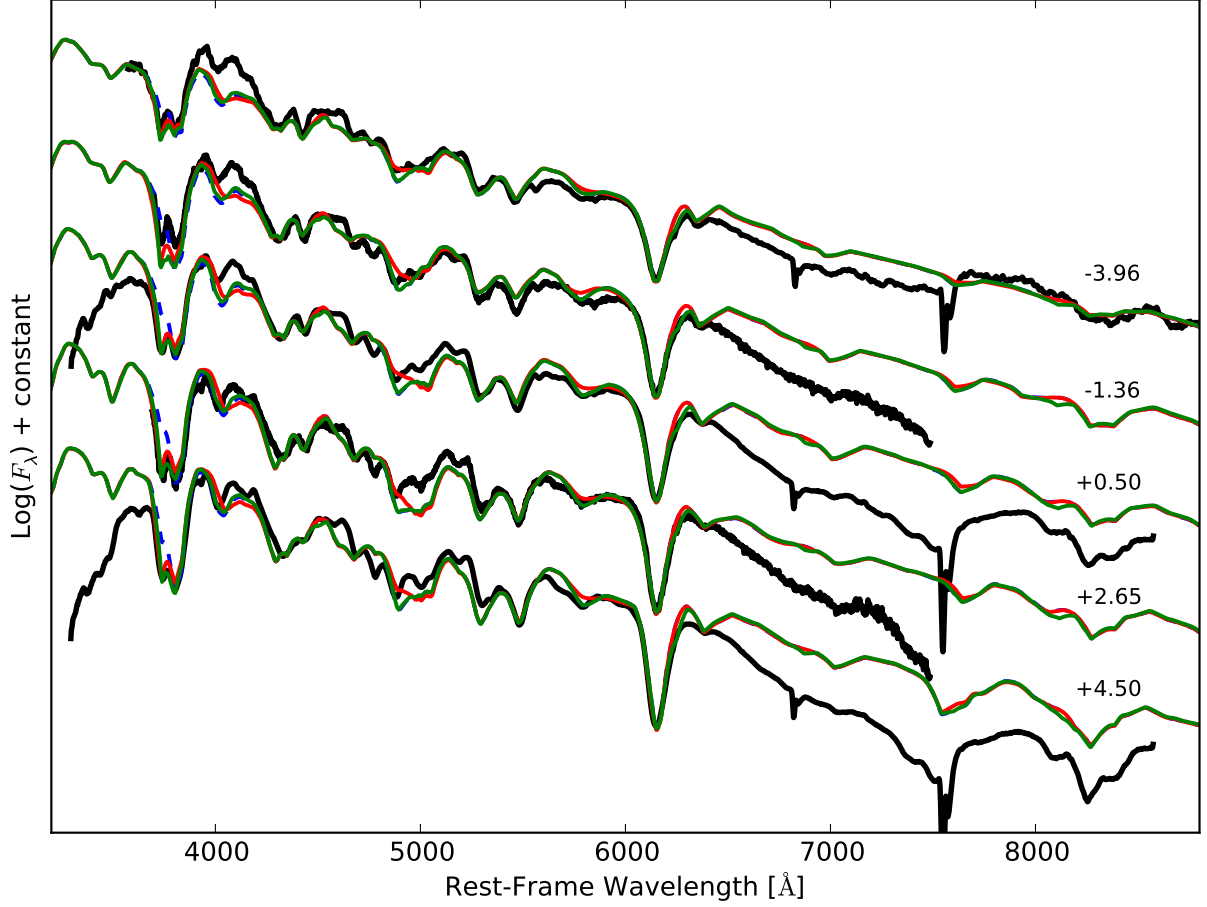


Fig. 16.— SYN++ models of the observed spectra of SN 2002fk spectra, shown in black. We show the same models as in Figure 14 but for the full spectrum for representative phases. The phase of the spectra is on the right side.

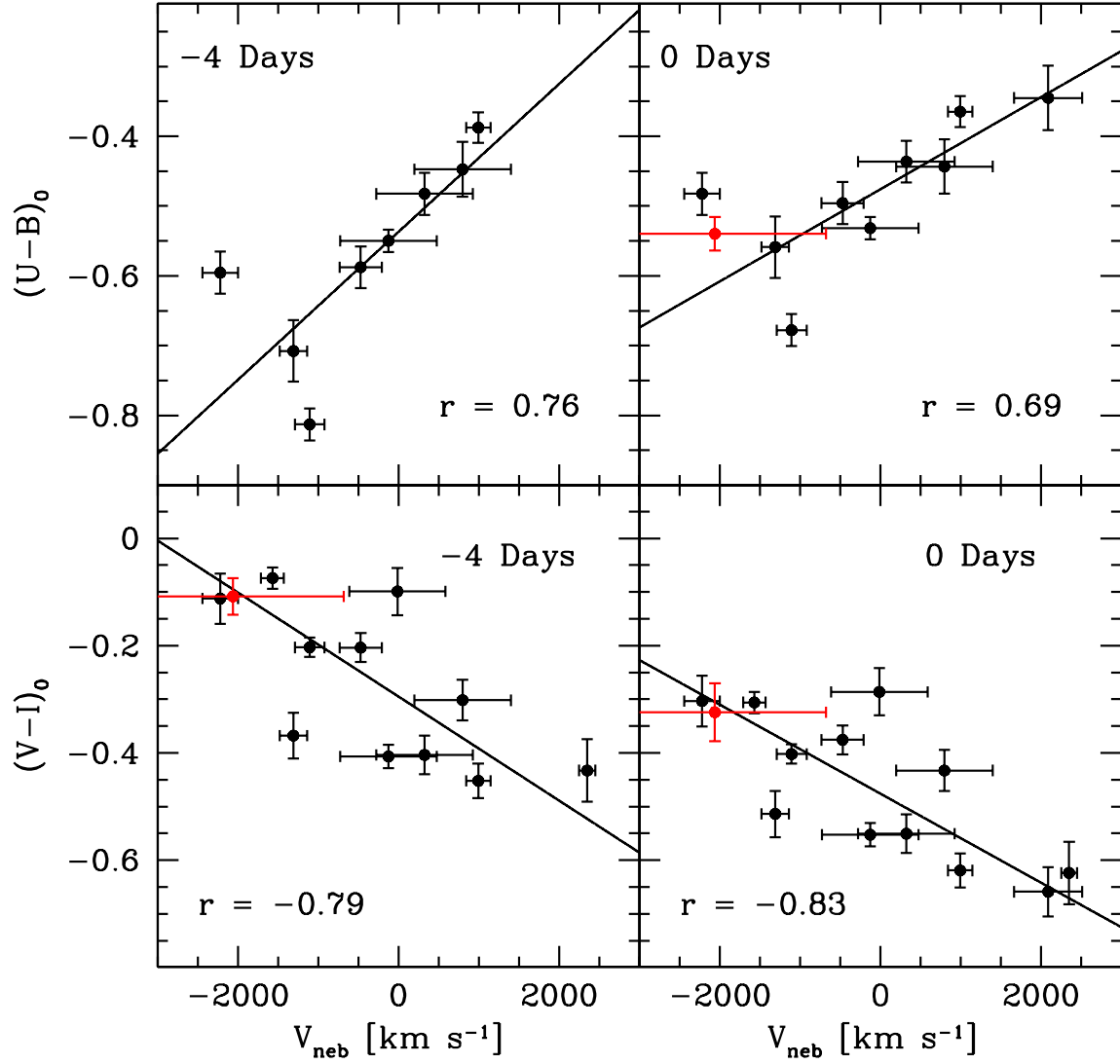


Fig. 17.— Figure 2 of Cartier et al. (2011). In top panels are shown $U-B$ reddening corrected colors vs. V_{neb} , in the bottom panels are plotted $V-I$ reddening corrected colors vs. V_{neb} . In red we show SN 2002fk which is in excellent agreement with Cartier et al. (2011) relations.